Applied Ocean Research 148 (2024) 104009

Contents lists available at ScienceDirect

Applied Ocean Research

journal homepage: www.elsevier.com/locate/apor

Research paper

An overtopping formula for shallow water vertical seawalls by SWASH

Sara Tuozzo, Mario Calabrese, Mariano Buccino *

Department of Civil, Architectural and Environmental Engineering, University of Napoli "Federico II", Via Claudio 21, 80125 Napoli, Italy

ARTICLE INFO

Keywords:
Wave overtopping
Shallow waters
Vertical seawalls
Numerical analysis
SWASH

ABSTRACT

There is now wide evidence that phase-resolving numerical models can capture the general physics of the overtopping process even under complex hydrodynamics. Based on this outcome, an extensive parametric study has been carried out with the model SWASH, to develop a design formula that uniformly predicts the overtopping rate at vertical seawalls for both breaking and non-breaking wave conditions. The use of the numerical model has allowed to vary the experimental conditions smoothly, avoiding the typical limitation of laboratory experiments. Furthermore, particular tests have been performed to assess whether, and up to which extent, the mean overtopping discharge is affected by the low frequency components of the incident wave spectrum.

The formula relates the overtopping rate to a new water level statistic, which represents the average of the highest one-fourth wave displacements at the toe of the wall; it has initially been derived for planar beaches and then extended to the case of slope varying foreshores. A comparison with an array of 200 laboratory experiments confirms that the new parametrization can reduce the scatter of data compared to the EurOtop equation.

List of symbols

A	scale parameter of beach equilibrium profile [$m^{1/3}$]
f	frequency [Hz]
f_p	deep water peak frequency [Hz]
g	gravitational acceleration [m/s^2]
h_{DEEP}	still water depth at the generation [m]
h_{TOE}	still water depth at the toe of the structure [m]
h*	impulsive waves parameter [-]
$H_{m0,DEEP}$	spectral wave height in deep water or at the generation [m]
$H_{m0,TOE}$	spectral wave height at the location of the structure [m]
$L_{m-10,TOE}$	spectral wavelength = $gT_{m-10,TOE}/2\pi$ [m]
$L_{p,DEEP}$	deep water wavelength = $gT_{p,DEEP}/2\pi$ [m]
m_n	n^{th} order spectral moment [m^2/s^n]
$m_{n,TOE}$	n^{th} order spectral moment at the toe of the structure [m^2/s^n]
$m_{0,low}$	wave energy below half f_p [m^2]
q	mean overtopping discharge per unit crest width [$m^3/s/m$]
q*	dimensionless mean overtopping discharge [-]
R_C	crest freeboard [m]
R_C*	dimensionless crest freeboard [-]
S(f)	power spectral density [m^2s]
tan(m)	foreshore slope
T_{m-10}	spectral wave period, based on m_0 and m_{-1} [s]
$T_{m-10,TOE}$	spectral wave period at the toe of the wall [s]
$T_{p,DEEP}$	peak period in deep water or at the generation [s]
Δx	horizontal grid dimension [m]
μ	mean wave elevation (i.e. wave setup or setdown) [m]
ζ_{TOE}	wave elevation time series at the location of the structure [m]
$\zeta_{1/4}$	average of the highest one-fourth of wave elevation distribution at the location of the structure [m]

1. Introduction

1.1. Background

Vertical seawalls are structural solutions very frequently employed to protect waterfronts and riparian properties along the shores (Allsop et al., 2005; Kraus and McDougal, 1996) that have long been researched through more than 50 years. Coastal engineers typically rely on these coastal defenses to prevent flooding, thereby reducing coastal risks.

One of the leading wave structure interaction processes is wave overtopping, which occurs when the water overcomes the crest and floods the backland. Due to its obvious impact on the life of coastal communities, wave overtopping is probably one of the most investigated hydraulic processes in coastal engineering, counting hundreds of publications dealing with it, and thousands of experiments carried out (CLASH, De Rouck and Geeraerts, 2005; EurOtop, 2018).

In modern engineering, the tools for the estimation of the

* Corresponding author.
E-mail address: buccino@unina.it (M. Buccino).

https://doi.org/10.1016/j.apor.2024.104009
Received 27 November 2023; Received in revised form 4 March 2024; Accepted 11 April 2024
Available online 17 April 2024

overtopping rate include empirical predictors and phase-resolving numerical models. The latter are physically based softwares that solve the equations of motion in a transient frame, and encompass Navier-Stokes solvers (either Eulerian or Lagrangian) and models based on the long wave approximation (Shallow water equations or Boussinesq waves). The models differ in degree of complexity and computational times; a systematic comparison of their performance has been recently carried out by Buccino et al. (2023); among other major numerical studies on wave overtopping are those of Altomare et al. (2021), Chen et al. (2021), Suzuki et al. (2017), Tonelli and Petti (2013), Losada et al. (2008).

Empirical predictors can further be split into machine learning techniques, which exploit the availability of large databases (Zanuttigh et al., 2016; den Bieman et al., 2021), and the traditional regression formulae, which this article pays particular attention to. It will be shown, in fact, that the look for robust predictive equations still deserves additional efforts, especially in very and extremely shallow water scenarios (Hofland et al., 2017).

An in-depth review of the literature reveals, in effect, two different approaches to the formulae, which distinguish themselves by the hydraulic variables employed as predictors. The first uses low exceedance water level statistics, namely the extreme run-up heights; therefore, the wave overtopping process is related to another wave-structure interaction phenomenon (wave run-up). This approach has been used in several works, such as de Waal and Van der Meer (1992); Hedge and Reis (1998); Mase et al. (2013), Yuhi et al. (2020), Ibrahim and Baldock (2020), and Etemad-Shahidi et al. (2022). The resulting methods, though, suffer from a number of drawbacks, including uncertainties about the most reliable formula to calculate the run-up height (e.g. Hughes, 2004; Pillai et al., 2019; EurOtop 2018), and the need for iterative procedures and the estimation of leading quantities from graphs (see Mase et al., 2013).

On the other hand, the most agreed approach assumes the overtopping rate to be function of the moments of order -1 and 0 of the power spectral density at the location of the structures (EurOtop, 2018). The moments are used to calculate the spectral significant wave height $H_{m0} = 4\sqrt{m_0}$ and the harmonic mean period $T_{m-1,0} = m_{-1}/m_0$. Based on this idea, the following equations were developed by EurOtop (2018) for the specific case of vertical walls:

$$\frac{q}{\sqrt{g \cdot H_{m0,TOE}^3}} = 0.05 \cdot exp\left(-2.78 \cdot \frac{R_c}{H_{m0,\ TOE,}} \right) \tag{1a}$$

$$\frac{q}{\sqrt{g \cdot H_{m0,TOE}^3}} = \begin{cases} 0.011 \cdot \sqrt{\frac{L_{m-1,0}}{h_{TOE}}} \cdot exp\left(-2.2 \frac{R_C}{H_{m0,TOE}} \right) & for \ \frac{R_C}{H_{m0,TOE}} < 1.35 \\ 0.0014 \cdot \sqrt{\frac{L_{m-10}}{h_{TOE}}} \cdot \left(\frac{R_C}{H_{mo,TOE}} \right)^{-3} & for \ \frac{R_C}{H_{m0,TOE}} \geq 1.35 \end{cases} \tag{1b}$$

where q is the mean overtopping rate, R_C is the crest freeboard. Eqs. (1a) and (1b) refer to pulsating ($h^* > 0.23$) or impulsive ($h^* \leq 0.23$) loadings, respectively; the parameter h^* indeed discriminates between breaking and non-breaking wave conditions:

$$h^* = 2\pi \cdot \frac{h_{TOE}}{g T_{m-1,0}^2} \cdot \frac{h_{TOE}}{H_{m0,TOE}} = \frac{(h_{TOE})^2}{L_{m-1,0} \cdot H_{m0,TOE}} \tag{2}$$

It is worth specifying that the coefficients in Eq. (1) represent the average value of the stochastic parameters, according to the mean value approach of the EurOtop Manual. From a closer inspection of the formulae, it is surprising that the wave period does not affect the overtopping rate in relatively deep water, just when the spectrum features a clear peak frequency; on the other hand, it does in shallow water, when the spectral shape becomes complex. In addition, the presence of a sharp boundary between quasi-static and impact conditions introduces some further uncertainties.

Nevertheless, the main drawback in the EurOtop formulae is that the prediction of the spectral moments can be challenging in a surf-zone, particularly for m_{-1}, since the occurrence of InfraGravity waves (IG) of "surf beats" (Tucker, 1950) carries a considerable amount of energy below the peak of the incoming seas (e.g. Symonds et al., 1982; Shaffer, 1993). In these cases, EurOtop suggests estimating the wave parameters using phase-resolving models.

Since this procedure is certainly lengthy, following the approach of Goda et al. (1975), Lashley et al. (2021) proposed a set of design formulae that allow to calculate q directly from the offshore climate. The method was originally developed for planar beaches and has recently extended to the case of real beach based on field data (Lashley et al., 2023). Anyhow, predictions from offshore wave parameters presume regular topographic conditions and are therefore less general compared to the use of "toe" quantities.

1.2. Scopes of the work

This research can be viewed as the natural prosecution of the recent article of Buccino et al. (2023). The authors have analyzed the overtopping of a vertical seawall in an uneven surf-zone, based on both physical and numerical model tests; in particular, the numerical experiments were carried out with phase-resolving models with different degrees of complexity, namely CFD-RANS and the model SWASH, which exploits the Non-Linear Shallow Water (NLSW) equations extended with a non-hydrostatic pressure term. The major conclusions of the article can be summarized as follows:

1. The EurOtop database for vertical walls includes practically no reliable data of seawalls in the inner surf-zone. In particular, the spectra featured no or very few surf-beats and, accordingly, the mean harmonic period in Eqs. (1b) accounts for no effects other than the peak period in deep waters;
2. $T_{m-1,0}$ does not actually influence the overtopping rate, but due to a spurious correlation effect caused by its proportionality with H_{m0}.
3. The overtopping rate is well predictable in the function of a water level statistic, related to the upper tail of the distribution of wave displacements at the toe of the wall.
4. Although producing some underpredictions of q, SWASH was found to capture the general physics of the process satisfactorily well.

Moving from those findings, in this article, we first use SWASH to gain a deeper insight into the relationship between mean overtopping discharge and the Fourier power spectrum, which, as mentioned, is central to engineering applications. Then, the model is used to develop a robust design equation, which predicts the overtopping rate at vertical seawalls in a wide range of hydraulic, structural and topographic conditions. The use of a numerical model allows the experimental conditions to vary smoothly without the typical limitations of physical models. The final formula is eventually compared with 196 laboratory experiments, including those of EurOtop's "reliable" database. A trustworthy predictive model is essential since the mean overtopping discharge, along with the maximum individual volume, is the hydraulic parameter necessary for designing sea defenses.

1.3. Outline

The article is organized as follows: the main characteristics of the numerical model can be found in section 2, while the structure of the experimental campaign is described in section 3. Section 4 shows the obtained results; in particular, section 4.1 compares time and frequency domain variables related to the overtopping process, whereas sections 4.2 and 4.3 show the new proposed formula gathered from numerical data, and its re-calibration based on laboratory tests. Finally, section 5 and 6 provide, respectively, a discussion on the obtained results and the main conclusions of this work.

2. Numerical model SWASH

SWASH (acronym for Simulating WAves till SHore) is an open source time domain wave model that ensures to analyze a variety of coastal phenomena (Zijlema et al., 2011); indeed, it has been designed to study propagation of dispersive surface waves from offshore to the shore, surf zone and swash zone dynamics, wave agitation in ports, and coastal-structure interactions.

2.1. General features

SWASH is a non-hydrostatic phase-resolving model that integrates the Non-Linear Shallow Water equations extended with a non-hydrostatic pressure term. Along with the global balances of mass and momentum in the horizontal direction for a depth-averaged, non-hydrostatic, free-surface flow, the governing equations include a local continuity equation and a simplified local momentum balance in the vertical direction (see Smit et al.,2014; Zijlema et al., 2011; Zijlema and Stelling, 2008). Thus, the numerical model is able to properly reproduce the wave shoaling, refraction, and breaking phenomena.

Such a non-hydrostatic model assumes a single-valued representation of the free surface in the horizontal plane, $\zeta(x,y,t)$, which means that the compute of free surface flow requires no additional treatment methods. This enhances the computational efficiency, although prevents the model reproducing complex processes such as overturning, air-entrainment, and the production of wave-induced turbulence after the incipient breaking.

It is worth to emphasized that SWASH may be run either in depth-averaged mode or in multi-layered mode, i.e. the computational domain is vertically divided into a fixed number of layers. The latter ensures that the vertical structure of the flow is in a way part of the solution. The higher the number of layers, the better the dispersive properties, in contrast to Boussinesq-type models' approach that improves frequency dispersion by increasing the order of derivatives in the governing equations. However, the use of the Keller Box scheme (Lam and Simpson, 1976) to handle the pressure gradients in the vertical momentum equation guarantees good dispersive properties even at low vertical resolution. Simultaneously, the Hydrostatic Front Approximation (HFA) developed by Smit et al. (2013) allows an appropriate reproduction of the bulk characteristics of wave breaking when few layers are employed. The HFA indeed ensures that, during the breaking, vertical accelerations are no longer resolved and the non-hydrostatic pressure is set to zero – the governing equation are locally reduced to the classical NLSW equations.

Finally, SWASH adopts an explicit, second order accurate finite difference method for staggered grid that conserves both mass and momentum at the numerical level, and a second-order leapfrog scheme for time integration (Hansen,1956), with an adaptive time step that satisfies the Courant-Friedrichs-Lewy stability condition.

2.2. Coastal processes modeling via SWASH

Over the last decade, the numerical model developed by Zijlema et al. (2011) has been increasingly used to analyze wave-structure interaction processes (e.g. Suzuki et al., 2017; Gruwez et al., 2020; Zhang et al., 2016; Zhang et al., 2020; Buckley et al., 2022). Suzuki et al. (2023) have dealt with wave overtopping in port environments; a comparison with physical model tests has shown the capability of SWASH to predict the mean overtopping discharge with both perpendicular and oblique incident waves. Henderson et al. (2022) have validated the estimation of run-up and number of overtopping events with field observations of an extreme event. The authors have obtained consistent results between numerical and field data, although the overtopping events have been overestimated by a factor of 2. Lerma et al. (2016) have investigated SWASH performance with different model configurations in reproducing wave set-up and run-up on a complex barred beach on the French coast. In particular, the study has pointed out that the 2D mode of SWASH might be more suitable to investigate coastal processes; indeed, 1D configuration tended to overestimate set-up and run-up field data as it neglected some three-dimensional phenomena (e.g. alongshore wave-induced rip current). Several studies have focused on the wave overtopping modeling of sloping dikes with very shallow foreshores (see Suzuki et al., 2014; 2011); among them, Suzuki et al. (2017) represents one of the most essential work. The authors accomplished an extensive and detailed analysis about the estimation of wave overtopping in shallow water by numerically reproducing 124 tests from four different physical model campaigns. Both wave evolution and overtopping have been carefully examined, as the authors stated that an accurate estimation of the mean overtopping discharge requires a good reproduction of the incident wave properties. Then, the suitability of SWASH to predict the flow rate in very shallow waters has been proved, although the model performances worsen as the discharge decreases. Recently, Buccino et al. (2023) have employed the non-hydrostatic model to investigate the wave overtopping on vertical walls in shallow waters along with the relationships between the flow rate and incident wave characteristics; as mentioned above, the analysis involves both numerical and laboratory data on a multi-slope beach. Beyond the mere validation, the authors have analyzed the model's capabilities to describe the physics of wave transformation and overtopping in depth. Results have demonstrated that, as much as the RANS model, SWASH is able to describe the correlations relating to spectral moments within the surf zone and the relationships between the overtopping rate and the wave properties at the toe of the wall.

However, although the literature has gathered satisfactory validations of the numerical model, SWASH experiences some biases concerning wave transformation and overtopping. Indeed, despite the non-hydrostatic model well captures the dominant features of the spectral evolution from deep waters up to the shore, it tends to overestimate wave energy at high frequencies. This behavior has been underlined in Buccino et al. (2023), but has already been noticed in Zjilema et al. (2011) and Zjilema and Stelling (2008), where two different laboratory experiments of Boers (1996) were reproduced. Even if two types of foreshore – a multi-slope and a mild barred beach, respectively – and different wave steepness values have been involved, the studies agree that the energy is well reproduced at low frequencies and overpredicted at higher. Nevertheless, such bias does not seem to be systematic. Suzuki et al. (2017) indeed observed a fairly good agreement between numerical and laboratory outcomes on the steeper foreshore investigated ($tan(m) = 1/35$), while an underprediction of wave energy along the entire bandwidth has been obtained with the 1/50 slope. On the other hand, the tendency of SWASH to systematically underestimate the mean overtopping discharge has been established by several studies (Buccino et al., 2023; Lashley et al., 2020b; Suzuki et al., 2017; Suzuki et al., 2011).

Although some biases have been found, a large amount of studies has ascertained the reliability of SWASH in modeling wave-structure interaction phenomena. Hence, based on its validity largely proved by the literature, some researchers have employed SWASH in an exploratory way. Suzuki et al. (2020) have investigated the overtopping related variables (e.g. flow thickness and velocity) that affect human safety, since the numerical model facilitates challenging measurements compared to the laboratory. Nguyen et al. (2020) have adopted SWASH to analyze the spectral wave evolution and the overtopping at dikes on very gentle foreshores ($tan(m) > 1/250$) that have never been investigated during physical experimental campaigns.

Overall, such a non-hydrostatic model is characterized by some attractive peculiarities concerning numerical modeling. First of all, no treatments (e.g. VOF) are required to track the free surface motion as it is described by a single-valued function of the horizontal plane; moreover, few grid cells are necessary to represent the vertical structure of the motion. Hence, its inherent trade-off between correctly reproducing

wave-related phenomena and saving computational costs has ensured that SWASH can compete with more sophisticated phase-resolving models, such as CFDs. Therefore, the non-hydrostatic model is an optimal tool to deepen the analysis of wave overtopping of seawalls in shallow waters.

3. Experimental campaign

Numerical experiments have been executed via SWASH to analyze the overtopping phenomenon in shallow waters. Based on the results of Buccino et al. (2023), the present study aims to explore the hydraulic variables that truly influence the overtopping process and finally to find out a more appropriate formulation to estimate the mean overtopping discharge at vertical walls under both impulsive and non-impulsive loadings. To this end, the experimental campaign was organized into two phases.

Firstly, we have performed ad hoc experiments to inspect the role of spectral shape on wave overtopping. This has been accomplished comparing the overtopping rate in response to wave oscillation signals that differ significantly in the frequency domain. These experiments are codified with "SSh" (Tables 2 and 3) and use random and periodic waves.

Then, the numerical outcomes of a second ensemble of tests (code NF) ensured to establish the new predictive formulation (Table 4). NF tests have been carried out on different beach profiles, so that three subsets can be distinguished: *NF_U* includes experiments on planar beaches, *NF_EP* refers to tests with convex beach bottoms (Brunn, 1954; Dean 1977) and *NF_MT* reproduces the multi-slope seafloor that characterizes the foreshore of the Malecòn Traditionàl (MT) of La Habana, Cuba (Cordova et al., 2015, 2016).

All the tests were previously carried out in the absence of the wall to infer the incident wave characteristics, both in the frequency and time domains. Overall, we performed 232 numerical experiments, the results of which are provided in tabular form as "*Supplementary material*".

3.1. Numerical setup

The numerical experiments have been conducted in a 1-D mode, using the non-hydrostatic correction.

At the up-wave edge of the numerical flume, a weakly reflective boundary condition is imposed, which radiates the waves propagating from onshore. Rear the vertical wall, a Sommerfield condition minimized wave reflection at the end of the channel.

The HFA approach (Smit et al., 2013) has been used to model wave breaking; the breaking parameters are set to the default values (i.e. $\alpha = 0.6$, $\beta = 0.3$). A zero value of the Manning coefficient has been used, which, according to Buccino et al. (2023), leads to values of the overtopping rates more consistent with laboratory measurements. The water depth has been divided into 2 layers; the horizontal discretization has guaranteed at least 70 points per nominal wavelength at the incipient breaking, L_{nb}, which is defined as $L_{nb} = \sqrt{gH_{m0,DEEP}}\cdot T_p$. Here we hypothesize that $H_{m0,DEEP}$ is of the same order as the incipient breaker height, H_b, and that, in turn, $H_b \cong h_b$. More details about the spatial discretization are shown in the Appendix I. The maximum Courant number assigned was 0.5.

3.2. Generation boundary conditions (G-BCs)

The wave generation boundary condition is set at the up-wave edge of the flume, along with the weakly reflective boundary condition. In this study, we use four different generation methods, as summarized in Table 1.

Periodic waves are generated through a cosine type inflow velocity signal that varies hyperbolically in the vertical direction (z). On the other hand, the JONSWAP BC employs the linear superposition of N harmonic components; the amplitude of each velocity component, u_n, is derived from the variance of the parametric spectrum (mean JONSWAP spectrum, Hasselmann et al., 1973), according to the linear wave theory. The related phase, φ_n is randomly selected instead (Zijlema et al., 2011).

Table 1
Summary of Generating boundary conditions.

Test-code	wave-type	G-BC	Duration (# T_p cycles)
SSh	periodic	cosine	50
	random	JONSWAP - BOUND	500
NF	random	JONSWAP – time series	500

The BOUND BC (Rijnsdorp et al., 2014) is based on the weakly nonlinear, second-order, finite-depth wave theory of Hasselmann (1962) that adds a second-order correction to the linear free wave's contribution:

$$u(x=0,z,t) = \sum_{n=1}^{N} u_n(z)\cos(2\pi f_n t + \phi_n) + \sum_{n=1}^{N} \times \sum_{m=n+1}^{N} u_{nm} cos[2\pi(f_n - f_m)t + (\phi_n - \phi_m + \pi)] \quad (3)$$

The second term on the right-hand side of Eq. (3) represents the contribution of the bound IG-waves forced by the difference interaction between the n^{th} and m^{th} free wave components (Longuet-Higgins and Stewart, 1962).

In 24 out of 30 *NF_MT* experiments, the waves are generated by providing SWASH with the incident wave elevation signals measured in the laboratory flume of the University of Napoli Federico II, during the experiments carried out to assess the overtopping of the *Malecòn Traditionàl* seawall (Còrdova et aL., 2015; 2016). The laboratory waves were generated by a piston-type wavemaker, using a linear random-phase (JONSWAP) generation method. Physical model tests were conducted at a scale of 1:30, while numerical tests are scaled-up to prototype. The periodic wave experiments lasted 50 peak period (T_p) cycles, while random wave experiments 500. According to Romano et al. (2015) 500 T_p cycles suffice to reach a stable value of the average overtopping discharge. However, the random wave tests conducted in the absence of wall (propagation tests) have a duration of 200 waves only.

Random wave spectra were estimated according to the Welch's method with a 0.003 Hz resolution frequency and 50% overlapping. In both periodic and random tests, a Hanning window was used to minimize the effects of spectral leakage.

3.3. SSh experiments

SSh includes 42 tests overall, which range from very to extremely shallow water based on the ratio $h_{TOE}/H_{m0,DEEP}$ (Hofland et al., 2017). Thirty-five were conducted on a planar beach inclined by 1/10 to the horizontal (*SSh_U*) and compare the behavior of random and periodic waves (Table 2). Further eight random wave experiments were carried out on the *Malecòn Tradicionàl* foreshore (Fig. 3), and are detailed in Table 3 with the code SSh_MT. These tests exploit two different generation BCs, namely JONSWAP and BOUND, allowing us to achieve wave spectra at the toe of the wall that differ only in the amount of surf beats.

Table 2
Summary of SSh_U. For periodic waves $H_{m0,DEEP} = (8\ m_{0,DEEP})^{0.5}$.

wave-type	G-BC	# tests	h_{DEEP} [m]	$H_{m0,DEEP}$ [m]	T_p [s]	h_{TOE} [m]	Rc [m]
random	JONSWAP	18	20.5	2.0 – 6.4	7 - 12	1.0	1.0; 2.0
periodic	cosine	16	20.5	1.4 – 5.9	5 - 12	1.0	1.0; 2.0

Table 3
Summary of SSh_MT.

Test - ID	G-BC	h_{DEEP} [m]	$H_{m0,DEEP}$ [m]	T_p [s]	h_{TOE} [m]	Rc [m]
SSh_MT 1	JONSWAP	20.45	7.2	12	3.43	2.23; 4.46
SSh_MT 2	BOUND	20.45	5.9	12	3.43	2.23; 4.46
SSh_MT 3	JONSWAP	20.45	6.7	12	3.43	2.23; 4.46
SSh_MT 4	BOUND	20.45	8.2	12	3.43	4.46

Such kind of comparison was not discussed before in the literature.

3.4. NF experiments

The NF phase encompasses 138 wave overtopping tests (Table 4). The experimental procedure considers different wall positions along the foreshore for *NF_U* and *NF_EP*, and a constant value of water depth at the toe of the structure, h_{TOE}, in *NF_MT*. The variation of h_{TOE} allows us to examine the wave overtopping of seawalls from shallow to extremely shallow foreshore conditions, whereas *NF_MT* includes tests in shallow and very shallow waters (Hofland et al., 2017).

3.4.1. NF_U. planar beach experiments

Three planar beaches have been investigated: a steeper foreshore inclined by 1/10 to the horizontal and two milder profiles characterized by tan*(m)* equal to 1/30 and 1/50. A flat bottom in front of the beach allows a proper development of the generated waves (Fig. 1a). The flat is long 180 m, which is approximately equal to one deep water (peak) wavelength of the longer wave investigated.

The location of the wall has been varied as well as the crest freeboard. Specifically, the variation of h_{TOE} led to overtopping tests in shallow waters ($h_{TOE}/ H_{m0,DEEP} = 1.4$, 2 and 2.7), very shallow waters ($h_{TOE}/ H_{m0,DEEP} = 0.5$ and 0.8) and extremely shallow waters ($h_{TOE}/ H_{m0,DEEP} = 0.2$ and 0.3). The crest freeboard has been raised from the ratio $R_C/ H_{m0,TOE} = 0.5$ up to 2 (Fig. 1b). Random sea states generated are characterized by a deep water wave steepness about 0.035. The hydraulic and geometric features are listed in Table 5.

3.4.2. NF_EP. equilibrium profiles experiments

The dataset *NF_EP* includes four different convex profiles, which are described by the power function of Bruun (1954) and Dean (1977). The peculiarity of such a profile lies in the variation of the local slope along the beach, which becomes steeper and steeper shoreward (Fig. 2). Furthermore, these takes the sediment size into account through the scale parameter *A*; thus, the coarser the sediment the greater *A*, that means a steeper beach. Overall, the use of different types of sediments allows us to consider both mild and steep profiles.

Specifically, we have investigated four different sediment sizes (d_{50} equals to 0.5, 1.8, 5, and 30 mm), related to sand and gravel beaches. The convex profile follows the Brunn-Dean equation up to the local slope relative to a water depth of 0.4 m; then, it reaches a berm crest of 2 m above the MWL with a uniform slope. The local slope range is 1/12 ÷ 1/85 and 1/7 ÷ 1/46 for the fine and coarse sand, respectively, while tan *(m)* = 1/4 ÷ 1/28 and 1/2 ÷ 1/15 for the two types of pebble beach.

The wave overtopping has been investigated in shallow, very shallow and extremely shallow foreshore conditions ($h_{TOE}/ H_{m0,DEEP} = 0.2 \div 2.7$). Two mean JONSWAP spectra characterized by $H_{m0,DEEP} = 2.4$ and 5.3 m and $T_p = 7$ and 10 s have been used (s_{0p} is about 0.03). The crest freeboard to incident wave height ratios varies between 0.5 and 1.5 ($R_C = 0.7 \div 5.6$ m).

Table 4
Summary of NF.

Dataset-ID	# tests	$H_{m0,DEEP}$ [m]	T_p [s]	$h_{TOE}/ H_{m0,DEEP}$
NF_U	63	1.3 – 5.3	5.3 - 10	0.2 – 2.7
NF_EP	45	2.4, 5.3	7, 10	0.2 – 2.7
NF_MT	30	1.7 – 6.5	5.5 - 14	- 2

3.4.3. NF_MT. The Malecon Tradicional experiments

Laboratory experiments carried out at the University of Naples "Federico II" in a 2D framework (Còrdova Lopez et al., 2015; 2016) have been numerically replicated at prototype scale using SWASH. The physical model campaign analyzed the wave overtopping of the Malecòn Tradicionàl, the vertical seawall that defend La Habana city (Cuba) against the flooding, and of others defense structures as well.

The La Habana foreshore has been approximated by a multi-slope beach profile (Fig. 3), which raised the seabed from 20.45 m below the MWL to the location of the Malecòn, namely -3.43 m. A flat area in front of the foreshore allowed the generated waves to develop properly. More details about the experimental layout can be found in (Còrdova Lopez et al., 2015;2016).

Eleven irregular sea states have been tested; 8 out of 11 use the “time series” G-BC, and correspond to the measurements taken at the laboratory flume of the University of Napoli Federico II. They encompass four target values of the significant wave height (2.5 m, 4.0 m, 5.4 m, and 6.5 m) and two peak periods (10 s and 12 s). The remaining seas generated with the JONSWAP BC aim to extend the analysis to different wave periods (5.5 s, 7 s and 14 s). The related significant wave heights ensure a deep water wave steepness about 0.035. Three different crest freeboards have been examined, namely 2.23 m, 2.73 m and 3.23 m above the MWL.

4. Results

4.1. Effect of spectral shape and water displacements on wave overtopping

Buccino et al. (2023) argued that the overtopping rate of a vertical seawall in the surf zone is scarcely affected by the shape of the incident waves’ spectrum and reasoned that the relationship between $T_{m\text{-}1,0,TOE}$, and q may result from a spurious correlation effect. Noteworthily, this does not challenge the role of IGs per se but rather the fact that one part or another of the variance spectrum (either in the low or high-frequency domain) might have a larger weight in determining the mean overtopping flux.

The authors reached their conclusions relying on pure statistical arguments, through the simple Added Variable Plot method (Draper and Smith,1998; Buccino et al., 2013). They analyzed numerical and physical model tests conducted on vertical seawalls and van Gent’s (1999) experiments on sloping walls.

In this section, we re-consider the above findings and try to test them most directly through experiments designed ad hoc (Tables 2 and 3). As mentioned, these exploit different generation BCs in SWASH to conveniently vary the wave spectra’ characteristics at the location of the structure.

4.1.1. Overtopping of random breaking waves with the same energy and different $T_{m\text{-}10}$ (SSh_MT tests)

JONSWAP and BOUND BCs can lead to different evolution paths for surf beats, even though the spectra at the generation boundary have the same energy and approximately the same shape. The experiments in Table 3 exploit this property to achieve wave spectra at the toes of the walls, which differ solely in terms of long-period wave energy. As an example, Fig. 4 compares *SSh_MT1* and *SSh_MT2*.

On the horizontal reach of the MT profile, the shape of the spectra is mostly similar (panel (a)), except for the low-frequencies where the second-order correction is applied. However, in JONSWAP waves, the energy below half the shortwave peak ($m_{0,low}$) remains less or very close to the Longuet-Higgins and Stewart (1962) theory (panel (b)), indicating

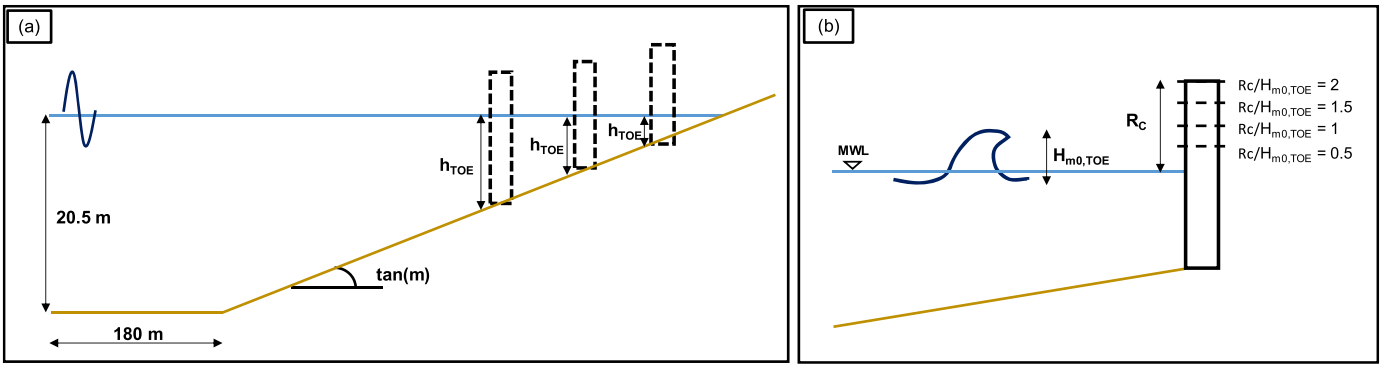

Fig. 1. Sketch of the experimental layout of dataset NF_U. Panel (a): schematization of the beach profile characteristics and the several water depths at toe of the wall investigated; panel (b): four different crest freeboard values examined for each wall position.

Table 5
Hydraulic and geometrical characteristics of NF_U.

tan(m)	# tests	$H_{m0,DEEP}$ [m]	T_p [s]	h_{TOE}/ $H_{m0,DEEP}$	R_C [m]
1/10	33	1.3 – 5.3	5.3 - 10	0.2 – 2.7	0.4 – 5.8
1/30	20	2, 5.3	7, 10	0.2 – 2	0.4 – 3.4
1/50	10	5.3	10	0.2 – 0.5	– 4.4

that the parasitic sub-harmonics associated with the linear generation (e.g. Barthel et al., 1983) do not affect the experiments significantly (more details are given in Appendix II).

When propagating through the foreshore (panel (c)), $m_{0,low}$ increases for both the sea states, either due to the development of phase-locked components or because of short-to-long wave energy transfer (e.g. Van Dongeren et al., 2007). However, the behavior radically changes in the surf zone.

The long wave energy of BOUND-generated waves decreases monotonically according to a dissipative trend (Rijnsdorp et al., 2014), suggesting the presence of an intense long-to-short (reverse) wave

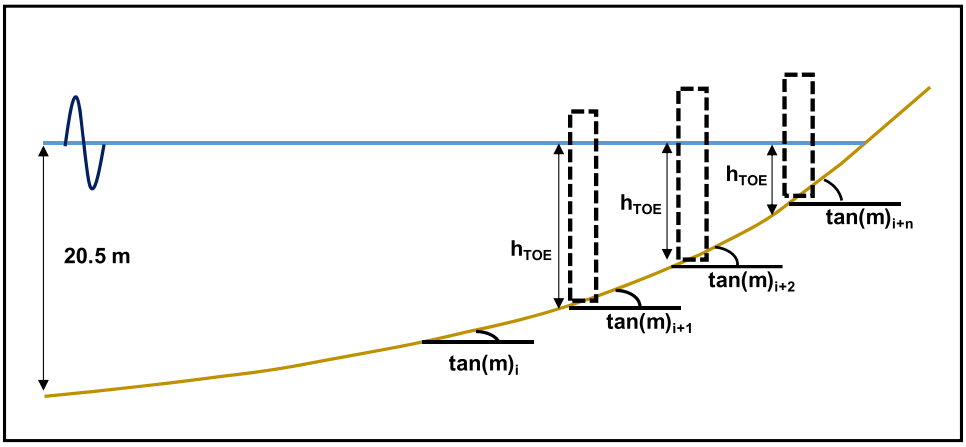

Fig. 2. Schematization of the investigated layout in NF_EP.

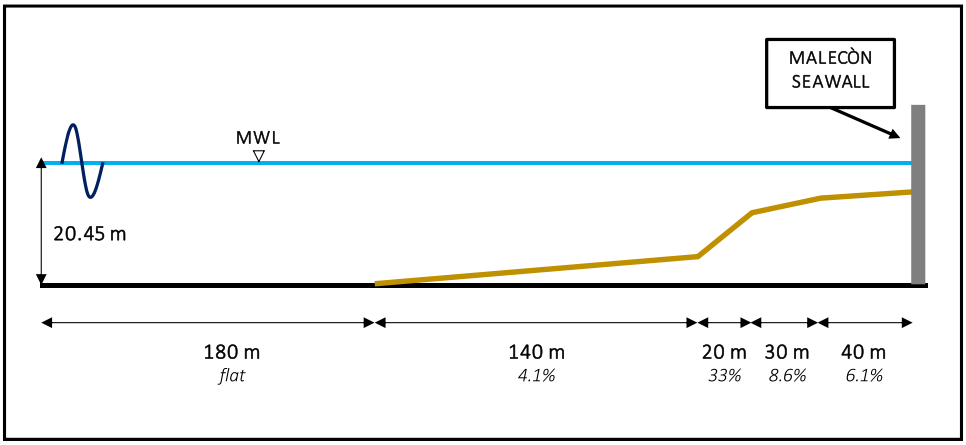

Fig. 3. Multi-slope foreshore of NF_MT (prototype scale).

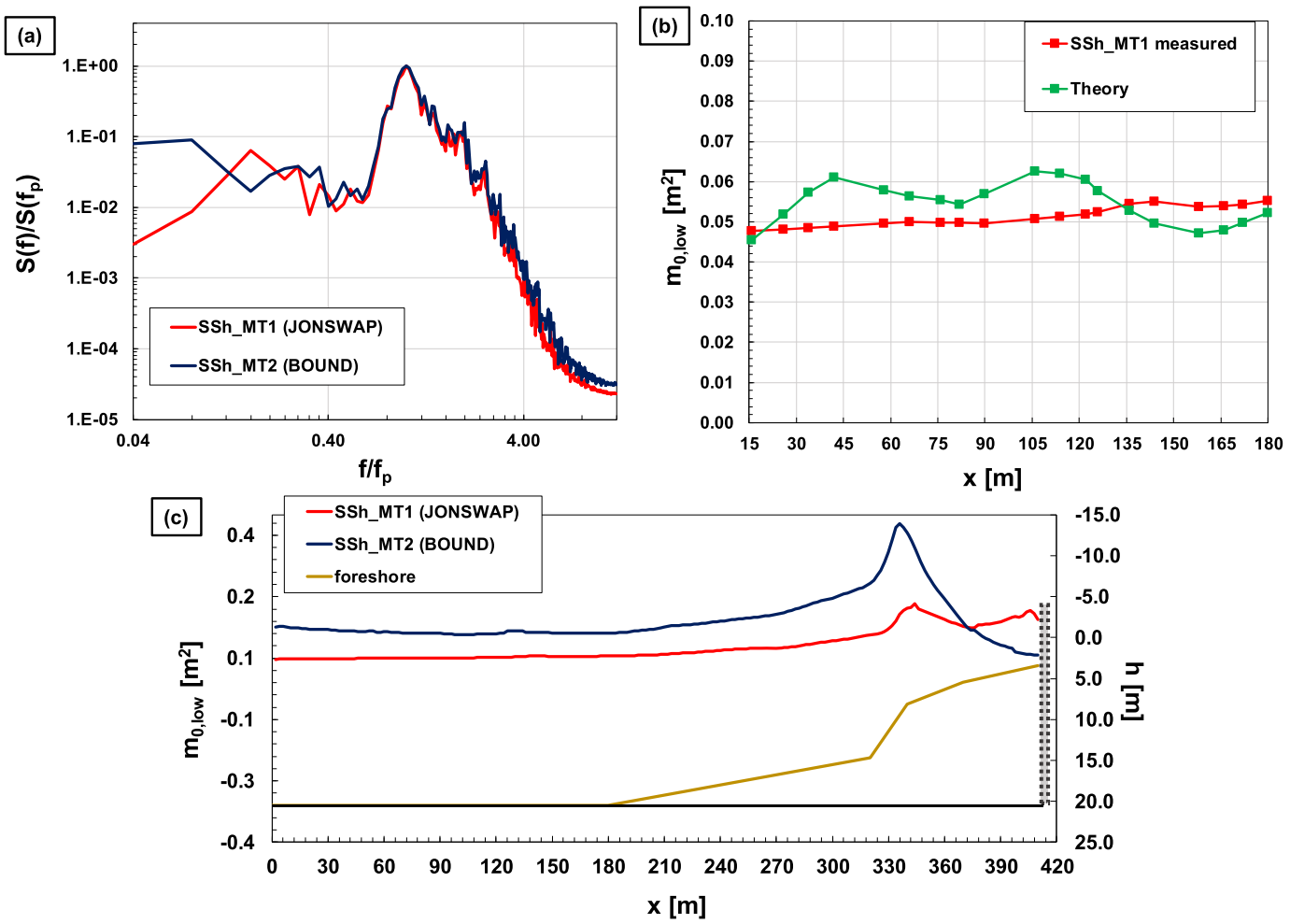

Fig. 4. Comparison SSh_MT1 and SSh_MT2. Panel (a) shows the non-dimensional wave energy spectra on the flat bottom (144 m far from the generation line); panel (b) compares the long wave energy of JONSWAP waves with the Longuet-Higgins and Stewart (1962) theory; panels (c) plot the long wave energy evolution along the MT profile.

energy flux (Bertin et al., 2018). In JONSWAP, on the other hand, $m_{0,low}$ tends to oscillate due to some extra forcings in the shallowest water; the analysis of the experiments suggests this behavior could be because these waves keep a more extensive envelope modulation after breaking. Most importantly to our scopes, however, both trends have already been observed in the literature (e.g., in Rijnsdorp et al., 2014 and van Doregen et al. 2007) and are therefore representative of real situations.

Heeding the previous discussion, Fig. 5 shows the spectra of the SSh_MT experiments at 3.43 m water depth, where we test the overtopping of two seawalls that differ in the height of the crest (2.23 m and 4.46 m).

The spectra have the same energy ($m_{0,TOE}$) and shortwave peak, but $T_{m-1,0,TOE}$ *varies significantly (40% in panels a) and c), and 80% in panels b) and d). The overtopping rate is systematically larger for the spectra with fewer IGs, which is in clear contrast to what one expected.*

4.1.2. Spectral shape and distribution of wave elevation (tests SSh_U)

The results observed in Fig. 5 are because in BOUND wave experiments, the fluctuations of the wave profile at the toe of the wall, ζ_{TOE}, reach higher levels than JONSWAP. As the wave variance $m_{0,TOE}$ is the same, this depends on quantities such as wave setup and wave skewness, which are inherently not reflected in the spectrum. Reasonably, then, the overtopping rate is mainly affected by the statistical distribution of the wave elevation, particularly the tail with low exceedance probability.

To provide further evidence, Fig. 6 compares random and periodic wave overtopping for two walls located at a depth of 1 m on a planar beach with $\tan(m) = 1/10$ (tests in Table 2). As a descriptor of the upper tail of the wave elevation distribution, the graph uses $\zeta_{1/4}$, i.e., the average of the highest one-fourth of the values of ζ_{TOE}. This statistic is defined as:

$$\zeta_{1/4} = 4 \int_{\zeta_{75}}^{\infty} \zeta_{TOE}\, f(\zeta_{TOE})\, d\zeta \tag{4}$$

in which f is the probability density function (pdf) of the wave elevation process, and ζ_{75} is the 75th percentile value.

Despite the dramatic difference in the spectral shape (Fig. 7), and periodic waves exhibiting no surf beats at all, the trends of the overtopping rate are remarkably consistent, even as the random wave energy shifts for the most part to the low frequencies (Fig. 7c and d).

4.1.3. $\zeta_{1/4}$ for linear (symmetric) waves

The use of $\zeta_{1/4}$ is in effect consistent with the approach adopted by many authors, who related the mean overtopping discharge to low exceedance run-up heights, such as $R_{2\%}$ (e.g. Hedge and Reis, 1998; Mase et al., 2013). It should be noted, however, that although it is likely related to, $\zeta_{1/4}$ is not a run-up statistic as it is calculated from the whole distribution of wave elevation at the toe of the wall (including negative values) in the absence of the structure.

An intriguing property of this quantity is a kind of invariance under

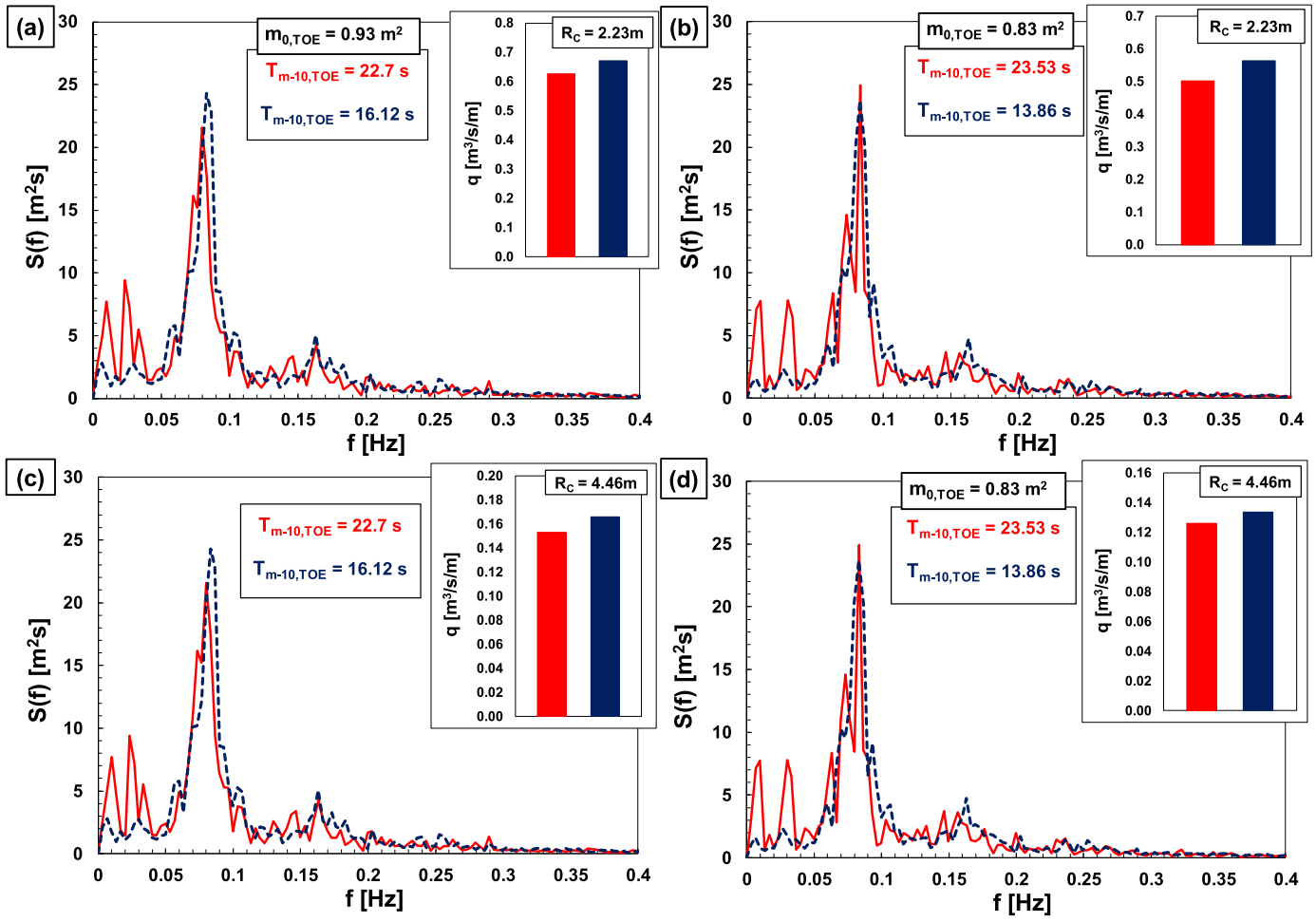

Fig. 5. Wave spectra at toe of the walls and overtopping rates for SSh_MT tests (red refers to JONSWAP sea states, while blue to BOUND generation). Panel (a): SSh_MT3 vs. SSh_MT4, R_C = 2.23 m. Panel (b): SSh_MT1 vs. SSh_MT2, R_C = 2.23 m. Panel (c): SSh_MT3 vs. SSh_MT4, R_C = 4.46 m. Panel (d): SSh_MT1 vs. SSh_MT2, R_C = 4.46m.

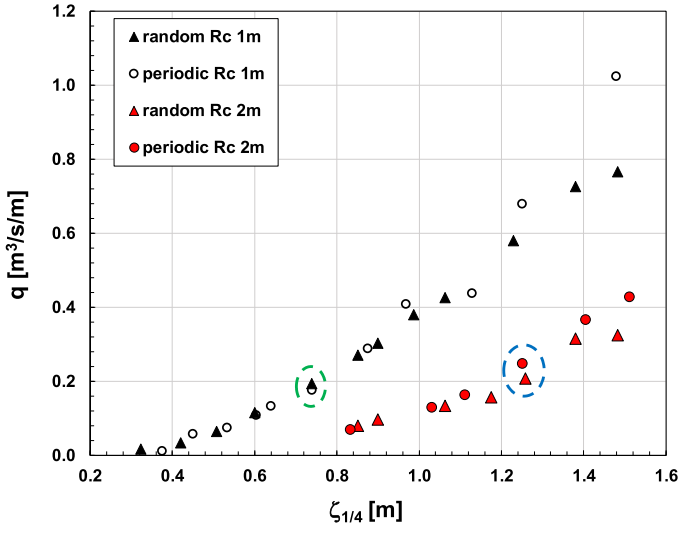

Fig. 6. The mean overtopping discharge as function of the average of the highest one fourth of wave displacements at the of the wall. Circles refer to wave spectra in Fig. 7.

linear waves. Indeed, as ζ_{TOE} is either a Gaussian random variable with variance σ^2:

$$f(\zeta_{TOE})_{gauss} = \frac{1}{\sqrt{2\pi\sigma^2}} exp\left[\frac{(\zeta_{TOE}-\mu)^2}{2\sigma^2}\right] \quad (5)$$

or a cosine signal with amplitude a:

$$\zeta_{TOE} = a\ cos(\omega t) \rightarrow f(\zeta_{TOE})_{cos} = \frac{1}{a\pi}\frac{1}{\sqrt{1-(\zeta_{TOE}-\mu)^2}} \quad (6)$$

Eq. (4) provides:

$$\zeta_{1/4} = \mu + 1.27\sigma = \mu + 1.27\sqrt{m_{0,TOE}} \quad (7)$$

where μ denotes the mean wave elevation, i.e., wave setup or setdown.

Unlike Fig. 6, which employs the entire time series at the toe of the walls, in the remaining part of this article we calculate $\zeta_{1/4}$ according to Eq. (7), and then neglect the effect of wave skewness. This approximation is assumed to be appropriate to the accuracy required by the engineering formulae for overtopping prediction.

4.2. A new formula for very and extremely shallow waters ($h_{TOE}/H_{m0,DEEP} \leq 1$)

The purpose of this section is to setup a relationship that predicts the mean overtopping rate at a vertical seawall in a surf zone, based on

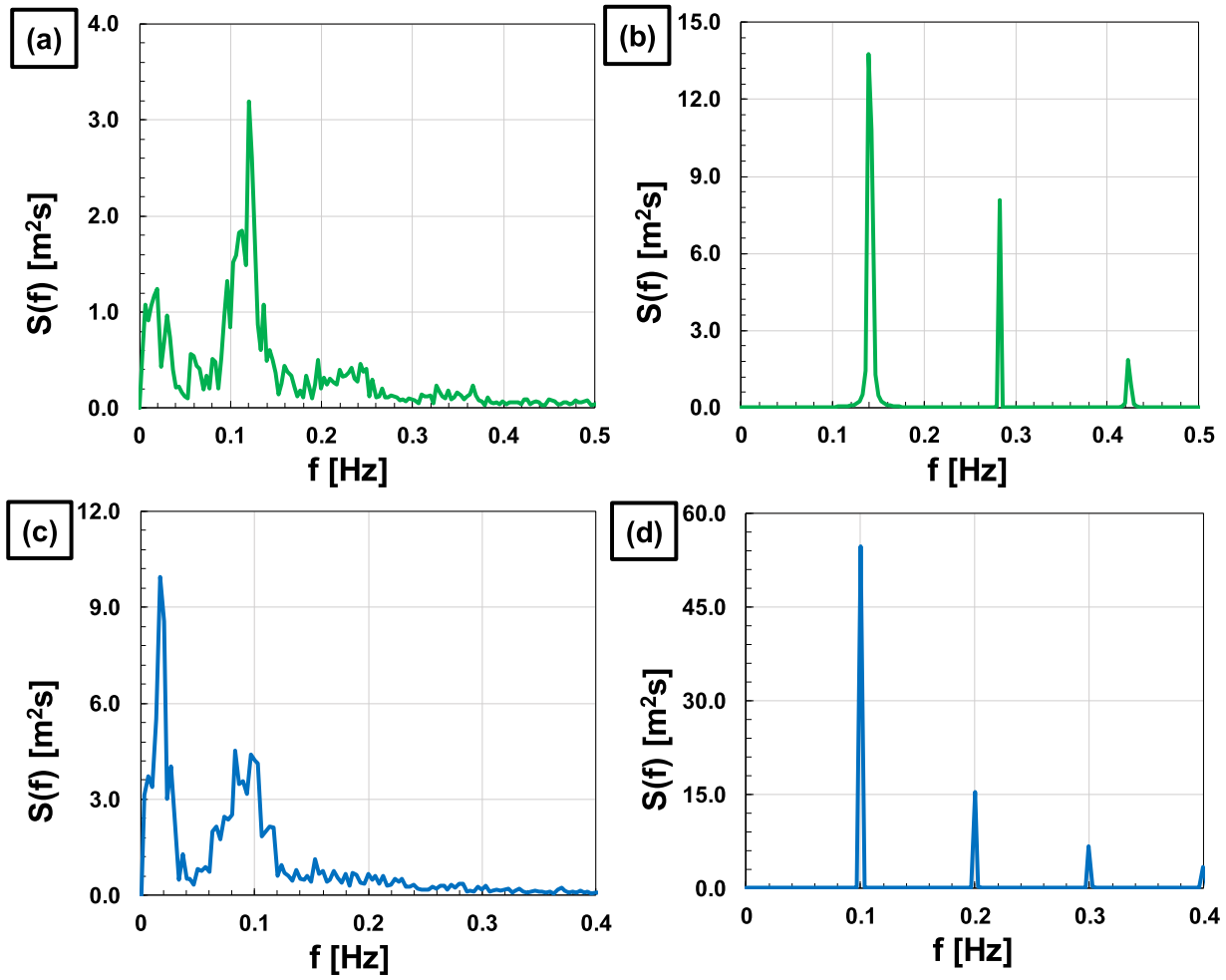

Fig. 7. Panels (a) and (b) illustrate the wave energy spectra at the toe of the structure of the random and periodic sea states circled in green in Fig. 6; analogously, panels (c) and (d) refer to the data circled in blue.

phase-averaged quantities only; these include the wave setup, μ, and the wave variance, $m_{0,TOE}$.

As usual, the formula will be relating a dimensionless flow rate q^* and a relative crest freeboard R_C^*:

$$q^* = F\left(R_C^*\right) \tag{8}$$

where the function F can be of either exponential or power type. For the crest freeboard we assume:

$$R_C^* = \frac{R_C}{\zeta_{1/4}} \tag{9}$$

where $\zeta_{1/4}$ is calculated according to the Eq. (7), as specified above.

As for q^*, it is convenient to refer to the EurOtop formula, which under very shallow waters conditions reads:

$$q^* = \frac{q}{\sqrt{g \cdot H_{m0,TOE}^3} \cdot \sqrt{\frac{t_{m-10}}{h_{TOE}}}} = \frac{q}{\left(g \cdot H_{m0,TOE} \cdot T_{m-10,TOE}\right) \sqrt{\frac{H_{m0,TOE}}{h_{TOE}}}} \tag{10}$$

It is worth noticing that the term in the round parentheses at the right hand side of Eq. (10) is in effect the reference flow rate used by Owen (1980) in his pioneering work.

Now we note that $T_{m\text{-}1,0,TOE}$ may be substituted by the offshore peak period $T_{p,DEEP}$. This for twofold reasons; on the one side, we the previous section has suggested that the effect of spectral shape on the overtopping process could be less than one may expect . On the other side, Buccino et al. (2023) have observed that the EurOtop reliable data for vertical seawalls all have $T_{p,DEEP}/T_{m\text{-}1,0,TOE}$ included between 0.9 and 1.2. Hence, the role of surf beats could not be assessed, and the variable $T_{m\text{-}10,TOE}$ is practically nothing else than the offshore peak period.

Furthermore, in a surf-zone we can set:

$$\frac{H_{m0}}{h_{TOE}} = \gamma(m) \tag{11}$$

in which m represents the slope of the foreshore. Therefore, Eqs. (8) and (10) lead finally to:

$$q^* = \frac{q}{g \cdot h_{TOE} \cdot T_{p,DEEP} \gamma(\mathrm{m})^{\frac{3}{2}}} = F\left(\frac{R_C}{\zeta_{1/4}}\right) \tag{12}$$

4.2.1. Uniform slope beaches: behavior of the new parametrization

Figs. 8a and 9a plot the dimensionless flow rate in the function of R_C^* (Eq. (9)):

$$q^* = \frac{q}{g \cdot h_{TOE} \cdot T_{p,DEEP} \cdot \tan(m)^{0.5}} \tag{13}$$

The 48 data of *NF_U* are remarkably well gathered and can be easily fitted with the following exponential function (Fig. 8a):

$$q^* = 0.031 \cdot \exp\left(-1.05 \cdot R_C^*\right) \tag{14}$$

to which corresponds an R^2 statistics of 0.97. The log-residuals of Eq. (14) are approximately Gaussian, as shown in Fig. 8b. Alternatively, a double power function can be used (Fig. 9a):

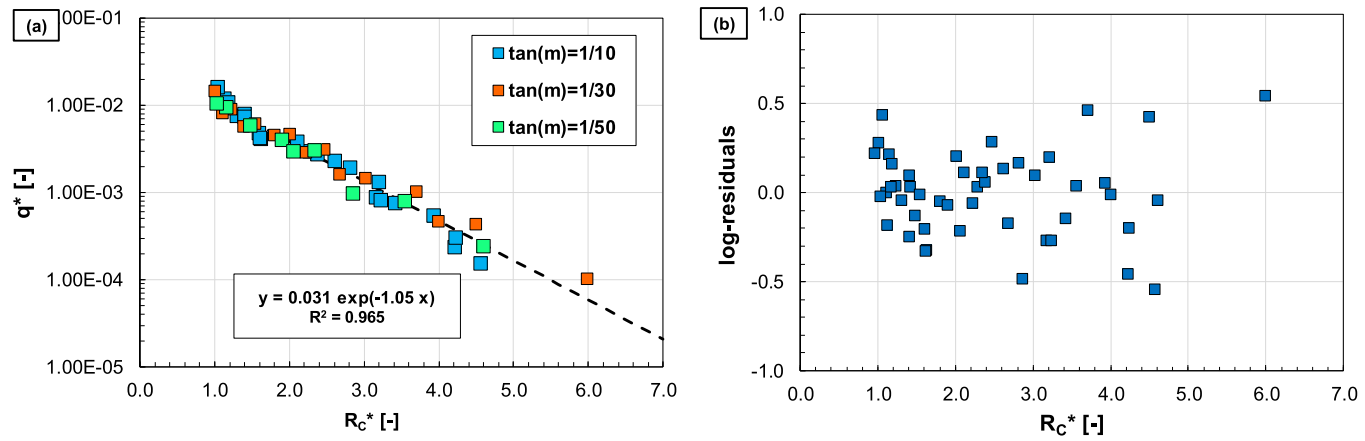

Fig. 8. Panel (a): planar beach data fitted by the exponential function; panel (b): log-residuals of Eq. (14) versus the predictive variable.

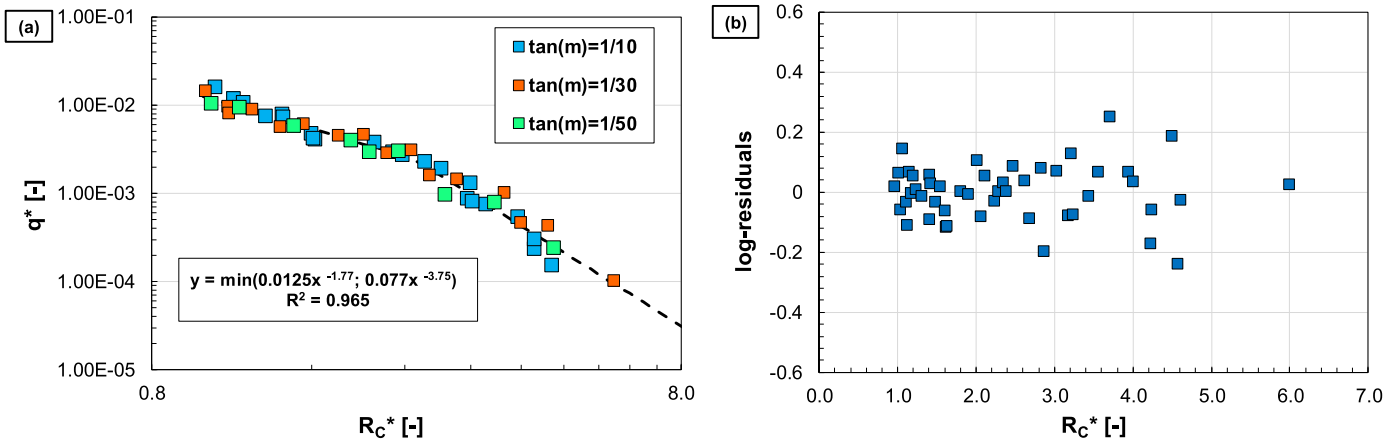

Fig. 9. Panel (a): planar beach data fitted by the double power function; panel (b): log-residuals of Eq. (15) versus the relative crest freeboard.

$$q^* = min\left[0.0125 \cdot R_C^{*\,-1.77}; 0.077 \cdot R_C^{*\,-3.75}\right] \quad (15)$$

with an R^2 statistics of 0.97. Fig. 9b shows no evident relationships between predictor and log-residuals, the behavior is quite homoscedastic. The valid range for Eqs. (14) and (15) is $1 \leq R_C^* \leq 6$.

It is worth noting that we have empirically observed a clear influence of the foreshore slope; indeed, although it has not been shown here for the sake of brevity, the presence of tan*(m)* in Eq. (13) avoids stratification of the data according to their own slope.

The parametrization used herein led to group the data far more efficiently than with the EurOtop formula, as can be appreciated in Fig. 10, where the 0.1 beach data are plotted on standardized graphs (by

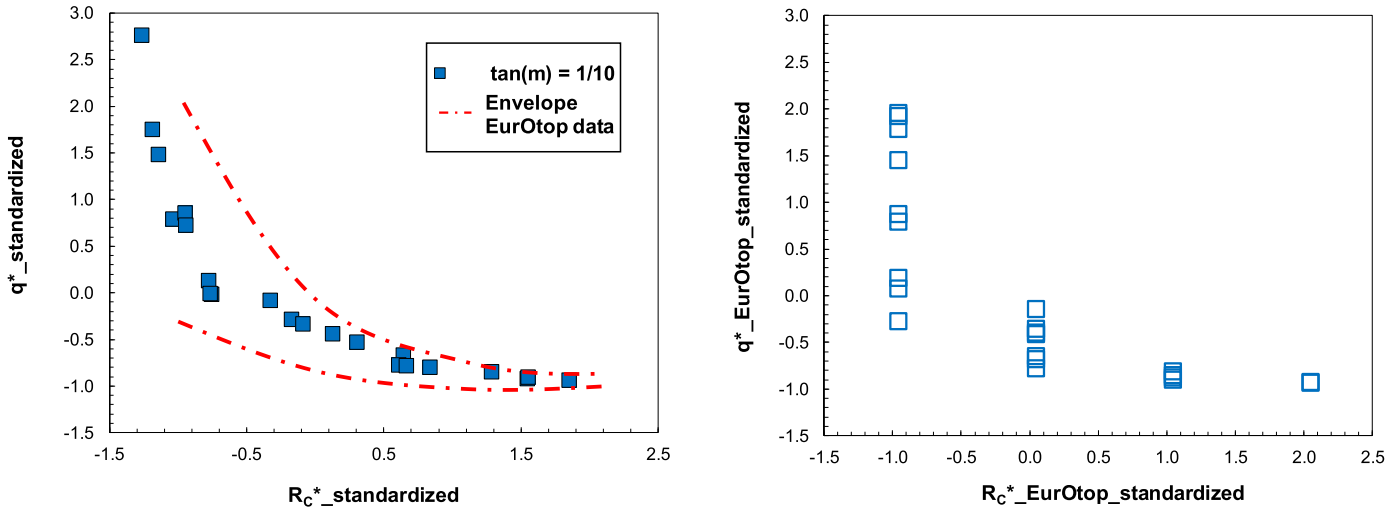

Fig. 10. Numerical data characterized by tan(m) = 1/10 are plotted on standardized variables. Panel (a): parametrization suggested in this paper, Eqs. (9,13). Data are compared to the envelope obtained using the EurOtop formulation shown in panel (b) as well.

subtracting mean from the variables and dividing by the standard deviation). This becomes even clearer by comparing our formulation with the envelope (red dash-dotted lines) derived from data in Fig. 10b.

4.2.2. A comparison with Lashley et al. (2021) formula

In this section, the overtopping rate predictions of the exponential formula, Eq. (14), are compared with those of Lashley et al. (2021) model in Fig. 11. Unlike the performance of Eq. (14), which guarantees that the 48 data of *NF_U* are quite close to the perfect agreement line, Lashley et al. formula provides contradictory results. Specifically, the comparison reveals a different behavior depending on the beach slope; indeed, numerical data for tan*(m)* = 1/10 agree fairly well with the Lashley et al. model, whereas significant underestimations occur as the beach becomes milder. In particular, a drop of linearity and correlation is observed.

Nonetheless, given the characteristics of the database used to calibrate their formula, this result is not really surprising. In fact, as shown in Fig. 9 of Lashley et al. (2021), the large part of data includes steeper beaches, while little information is available on beaches milder than tan *(m)* = 1/30. It is worth specifying, however, that higher underpredictions have been observed in the so-called "transition region", where the authors suggest an interpolation to estimate the mean overtopping discharge.

4.3. Extension to waves in shallow waters ($h_{TOE}/H_{m0,DEEP} < 4$)

In case of limited or very limited breaking, the condition of Eq. (11) is no longer valid. Thus, Eqs. (9) ad (13) need to be re-manipulated:

$$q^* = \frac{q}{g \cdot h_{TOE} \cdot T_{p,DEEP}} = \left(\frac{h_{TOE}}{H_{m0,TOE}}\right)^{-\frac{3}{2}} \cdot F\left(\frac{R_C}{\zeta_{1/4}}\right) \tag{16}$$

Hence, neglecting the effect of shoaling we may set the general relationship:

$$q^* = \frac{q}{g \cdot h_{TOE} \cdot T_{p,DEEP}} \cong F'\left(\frac{R_C}{\zeta_{1/4}}; \frac{h_{TOE}}{H_{m0,DEEP}}\right) \tag{17}$$

The formulation in Eq. (17) depends in practice only on the deep water climate, and should hold in general in the absence of breaking. Moreover, the beach slope angle does not appear among the variables.

However, the shift between breaking and non-breaking waves does not occur abruptly, but rather follows a transition law. Then we hypothesize the general function form:

$$q^* = \frac{q}{g \cdot h_{TOE} \cdot T_{p,DEEP} \cdot \tan(m)^P} \cong F'\left(\frac{R_C}{\zeta_{1/4}} \cdot \gamma_{br}\right) \tag{18}$$

in which the additional parameters γ_{br} and P depend on the degree of stability of the waves. Comparison with our data led to the following equations:

$$\gamma_{br} = \max\left[1; \frac{h_{TOE}}{H_{m0,DEEP}} \cdot tanh\left(10 \cdot \pi \cdot \frac{h_{TOE}}{L_{p,DEEP}}\right)\right] \tag{19}$$

$$P = \frac{0.5}{\left[1 + 50 \cdot exp\left(-10 \cdot \frac{H_{m0,DEEP}}{h_{TOE}}\right)\right]} \tag{20}$$

Therefore, as the wall is located in very or extremely shallow waters, γ_{br} =1 and P = 0.5; vice versa, in deep waters we have that $\gamma_{br} = h_{TOE}/H_{m0,DEEP}$ whereas P tends to 0.

In practice, for deepwater structures, the coefficient γ_{br} compensates empirically for the artificial reduction of non-dimensional flow rate caused by the increase of h_{TOE}; on the other hand, Eq. (20) takes into account that the wave motion in deep waters is not influenced by the characteristics of the seabed, including its slope. Altogether, Eqs. (19) and (20) accounts for the transition from pulsating to impulsive wave loadings, and are consistent with many studies conducted on vertical and sloping walls (e,g., Goda, 1995; Oumeraci et al., 1999; Vicinanza et al., 2015).

The whole subset *NF_U* (64 data) is plotted against the non-dimensional variables of Eq. (18) in Fig. 12a. The numerical outcomes are fitted properly by a double power function:

$$q^* = min\left[0.013 \cdot \left(\frac{R_C}{\zeta_{1/4}} \cdot \gamma_{br}\right)^{-1.89}; 0.024 \cdot \left(\frac{R_C}{\zeta_{1/4}} \cdot \gamma_{br}\right)^{-2.76}\right] \tag{21}$$

to which corresponds a R^2 value of 0.94. Fig. 12b plots the log-residuals that are randomly scattered, demonstrating the homoscedasticity of the model.

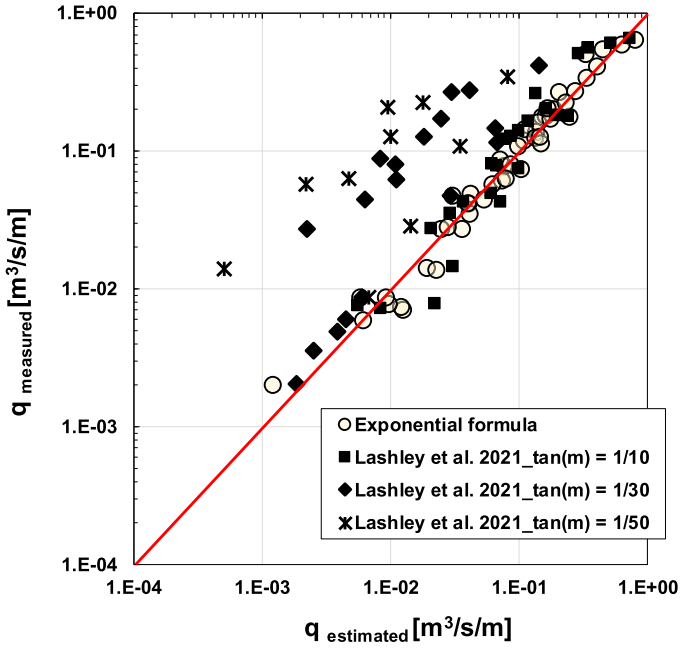

Fig. 11. Comparison between performances of Eq. (14) (circle points) and of Lashley et al. (2021) formula (black symbols). The red line represents the perfect agreement between measured and estimated flow rates.

4.3.1. Uneven slope beaches

The new function proposed in the previous section has been derived using planar beach data. However, real seabed is rarely so regular and exhibit a variable inclination instead. Thus, it is essential to define an equivalent slope required in Eq. (18) for the estimation of q.

To this end, we have examined the convex foreshores of *NF_EP* described in Section 3.2.2. In the analysis, we have evaluated four different approaches to define the equivalent slope for beaches characterized by irregular bathymetries. In Fig. 13, we have compared the predictive formula with the dimensionless flow rate obtained by using the four different equivalent slopes.

A common assumption is that of an averaged slope over a certain length (e.g. EurOtop, 2018). Hence, we suppose that the equivalent slope is averaged over some kind of distance $\mathscr{L}$ equals to either twice the local wavelength, $2L_p$, (Fig. 13a) or one deepwater wavelength, $L_{p,DEEP}$ (Fig. 13b). Then, according to the Bruun-Dean profile, for a given position x of the wall we have:

$$\overline{\tan(m)} = \frac{1}{\mathscr{L}}[y(x+\mathscr{L}) - y(x)] = \frac{A}{\mathscr{L}}\left[(x+\mathscr{L})^{\frac{2}{3}} - (x)^{\frac{2}{3}}\right] \tag{22}$$

In both cases, the wavelength is calculated considering the deep water peak period.

The third hypothesis (Fig. 13c) considers the hypothetical foreshore slope recently proposed by Lashley et al. (2023), which is a constant

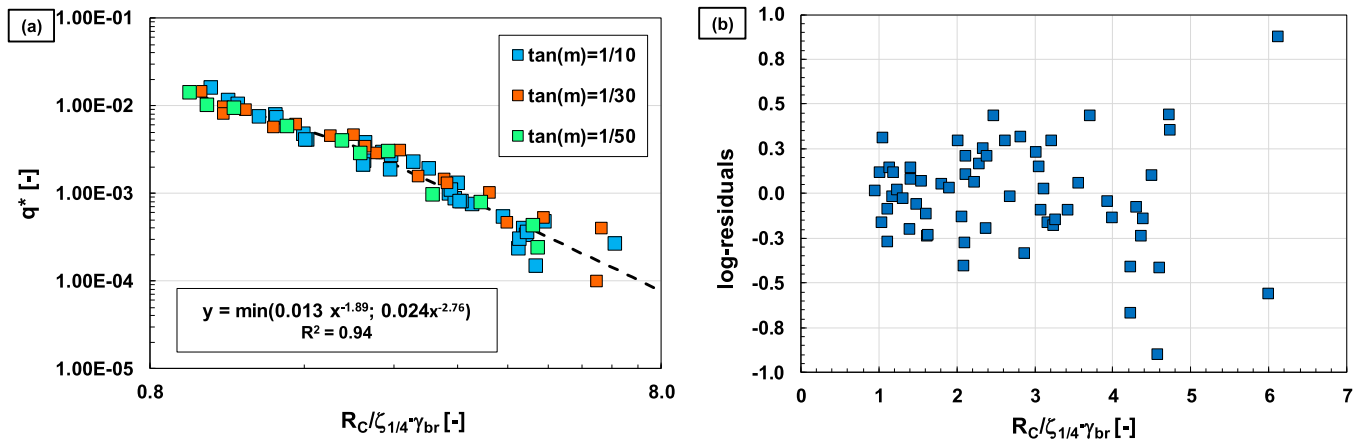

Fig. 12. Panel (a): the whole dataset NF_U fitted by the double power function; panel (b): log-residuals of Eq. (21).

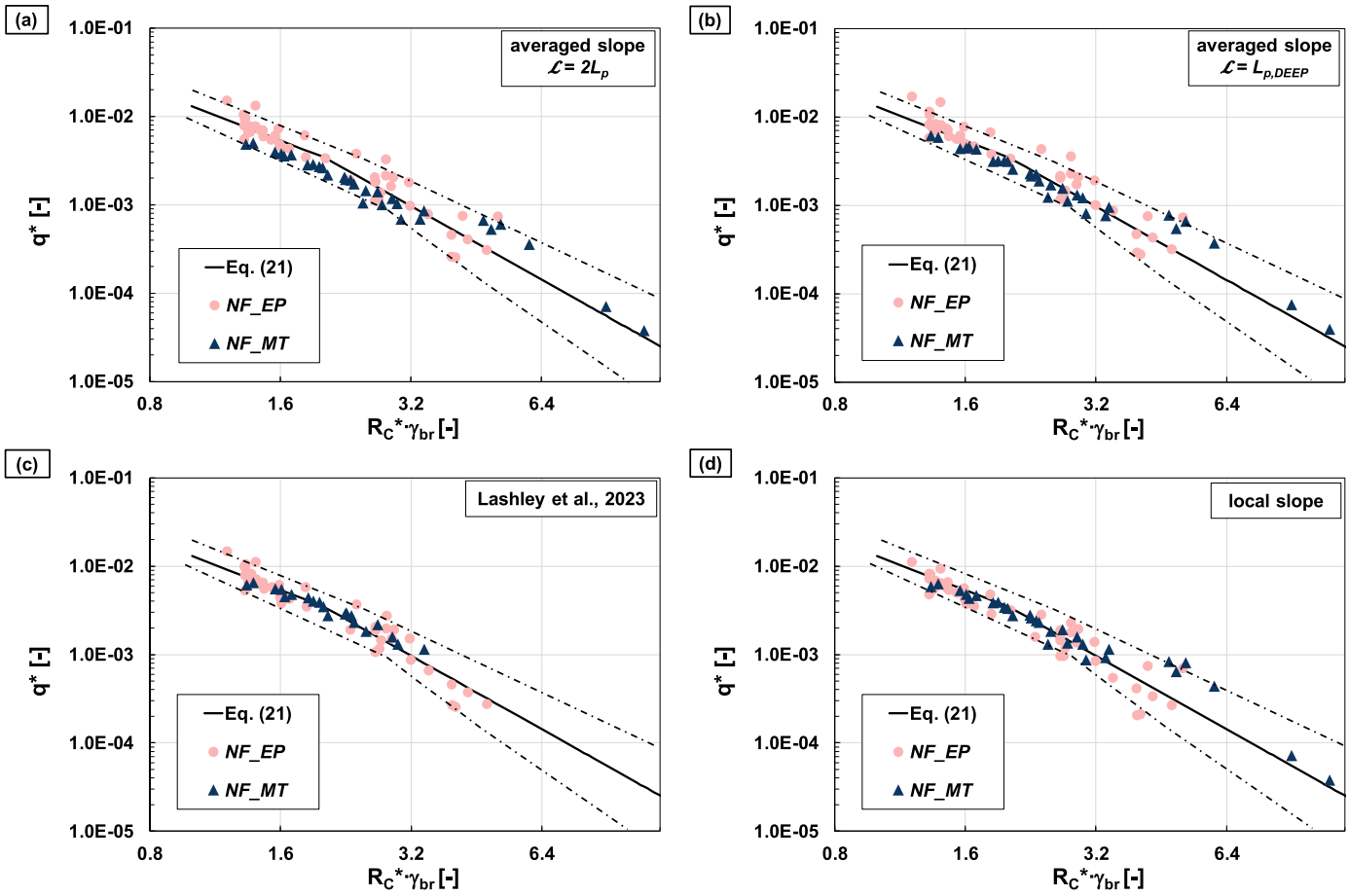

Fig. 13. Numerical data of NF_EP and NF_MT compared to the double power function (solid line) and the envelope of planar beach data, NF_U (dash-dotted lines). Panel (a) and (b) show the data obtained with the equivalent slope averaged on twice the local wavelength and on one deepwater wavelength, respectively; in panel (c) the hypothetical foreshore slope of Lashley et al. (2023) has been used; panel (d) depicts the data obtained with the local foreshore slope.

slope extending from a depth equal to $H_{m0,DEEP}$ to the toe of the structure (not applicable for seawalls located in shallow waters, $h_{TOE} / H_{m0,DEEP} \geq 1$).

Finally, the local foreshore slope at the toe of the wall has been examined (Fig. 13d), that for a convex profile described by the Bruun-Dean law reads:

$$\tan(m)_i = \frac{2}{3}\sqrt{\frac{A^3}{h}} \tag{23}$$

Furthermore, the multi-slope profile of *NF_MT* described in Section 3.2.3 has been considered as well. The four hypothesis explained above are applied on the Havana foreshore to derive the equivalent slope.

As shown in Fig. 13, no remarkable differences appear between the four options; indeed, the *NF_EP* and *NF_MT* data fall within the envelope of the planar beach dataset whether the equivalent slope adopted. However, Eq. (22) lead to a larger scatter for the convex profiles, regardless of the wavelength used, while the multi-slope foreshore data of *NF_MT* lie slightly beneath the predictive model curve, especially for

$\mathscr{L} = 2L_p$. On the other hand, both the local slope and the equivalent slope of Lashley et al. provide more satisfactory results; indeed, both the subsets are characterized by a little scatter and no significant biases are observed. These observations are quantitatively confirmed by the statistic indexes reported in Table 6; we have evaluated the outcomes of the four equivalent slopes compared to the estimates of Eq. (21) through the geometric mean, *Geo*, the geometric standard deviation, *GSD,* (see Goda, 2009) and the root mean square error, *RSME*. Overall, satisfactory performances have been obtained with both the local slope and the equivalent one proposed in Lashley et al., even if the latter cannot be applied on the entire datasets.

4.3.2. Comparison with laboratory data

As a final step of this study, we have verified our parametrization with the results of 194 laboratory tests that investigate wave overtopping at vertical walls, which include:

- 48 experiments conducted at University of Naples Federico II on the MT multi-slope profile (Cordova et al., 2015; 2016);
- EurOtop data for shallow and very shallow waters ($h_{TOE}/H_{m0,DEEP} < 4$) with a reliability factor RF = 1 and 2 (reliable and very reliable data). This array includes 146 data of both impulsive and non-impulsive conditions.

It should be noted that unlike MT, where all the information was available, EurOtop database does not provide the value of wave setup. However, as the ratio $h_{TOE}/H_{m0,DEEP}$ is larger than 0.82 for all test it has been realistically assumed to be zero.

Numerical outcomes appear consistent with laboratory data (Fig. 14a). Beyond a generalized underprediction, which was expected, physical model data lie almost wholly within Eq. (21)'s envelope bands. Moreover, impulsive and non-impulsive gather consistently.

Nevertheless, we obtained the best agreement between uniform and multi-slope profiles for $\mathscr{L} = 2L_p$. Although not representing the best match in numerical data, this equivalent slope yielded reasonable results also with SWASH (Fig. 13a).

The new parametrization leads to a scatter reduction compared to Eqs. (1), as can be appreciated in terms of standardized non dimensional variables in Fig. 14b. Note that for EurOtop we did not consider non-impulsive data, as they are predicted by a different formulation (Eq. (1a)). Overall, the observed behavior resembles that of numerical data in Fig. 10.

Finally, for practical use, we propose the following fit of laboratory data:

$$\frac{q}{g \cdot h_{TOE} \cdot T_{p,DEEP} \cdot m^P} = min\left[0.0107 \cdot \left(\frac{R_C}{\zeta_{1/4}} \cdot \gamma_{br}\right)^{-1.49}; 0.068 \cdot \left(\frac{R_C}{\zeta_{1/4}} \cdot \gamma_{br}\right)^{-3.04}\right] \tag{24}$$

to which corresponds an R^2 statistics of 0.94.

Table 6
. Statistic indexes that evaluates the performances of the four equivalent slope's investigated.

		# data	Geo	GSD	RMSE
averaged slope	*NF_EP*	45	1.103	1.415	1.62E-03
$\mathscr{L} = 2L_p$	*NF_MT*	30	0.864	1.438	9.87E-04
	Total	75	1.000	1.453	1.05E-03
averaged slope	*NF_EP*	45	1.168	1.389	2.00E-03
$\mathscr{L} = L_{p,DEEP}$	*NF_MT*	30	0.975	1.389	6.10E-04
	Total	75	1.086	1.407	1.60E-03
Lashley et al., 2023	*NF_EP*	42	1.018	1.354	1.42E-03
	NF_MT	20	1.027	1.141	4.54E-04
	Total	62	1.021	1.298	1.20E-03
local slope	*NF_EP*	45	0.917	1.406	9.35E-04
	NF_MT	30	1.087	1.422	4.78E-04
	Total	75	0.982	1.427	7.85E-04

5. Discussion

5.1. Spectrum shape and mean overtopping rate

The first part of this research has focused on the relationship between mean overtopping discharge and the Fourier spectrum of the incoming waves, which is a cornerstone in modern engineering prediction of wave overtopping. In this view, Section 4.1 discusses a few ad-hoc numerical experiments, in which the shape of the spectrum at the toe of the wall is conveniently varied by changing the wave generation boundary condition. The results essentially corroborate the conclusion of Buccino et al. (2023) that the statistical distribution of wave elevation, particularly the tail with low exceedance probability, affects the overtopping rate more significantly than the spectral shape. The average of the highest one-fourth of wave elevations, $\zeta_{1/4}$ (Eq. (4)), is in fact an efficient descriptor of this upper tail, and holds together regular and random wave data in Fig. 6, despite the energies being located dramatically different in the frequency domain. Also, $\zeta_{1/4}$ features an interesting invariance under linear waves (Eq. (7)), which makes it especially promising. In this context, the role of wave setup, μ, is peculiar, as it allows us to account for different evolution mechanisms in the surf-zone, such as in the case of planar and uneven foreshores.

The argument that the linkage between $T_{m-1,0,TOE}$ and q could be the product of a spurious correlation is also confirmed. To substantiate it, Fig. 15 shows two groups of experiments carried out on a slope of 1/10. The experiments are designed on different criteria; the left panels consider the random wave tests of Fig. 6, which feature h_{TOE} =1 m and a variable $H_{m0,DEEP}$. Instead, the right panels gather 9 data with the same wave conditions at the generation boundary but different water depths at the toes of the walls, as was in the experiments of van Gent (1999). For both groups, q increases with $H_{m0,TOE}$ (panels (a) and (b)), but the relationship between the latter and the harmonic wave period is the opposite. While in panel (c) $T_{m-1,0,TOE}$ correlates positively with $H_{m0,TOE}$, in panel (d) the relationship reverses. As observed in Buccino et al. (2023), this depends on how the experiments are designed, whether with h_{TOE} constant or variable. Anyhow, just as a consequence of these trends, we observe the overtopping rate increasing with $T_{m-1,0,TOE}$ in panel (e), and deceasing in panel (f). Noteworthily, the R^2 statistics of panels (a)-(e) and (b)-(f) are approximately the same.

However, the above does not intend to suggest that surf beats play no role in the overtopping process and can, therefore, be disregarded. More simply, we have found no reasons to argue that low frequencies have a particular weight in determining (just) the mean overtopping rate compared to, e.g., the shortwave components. Moreover, we have shown that accurate predictions of q can be achieved in shallow and very shallow waters, even when not considering $T_{m-1,0,TOE}$.

Of course, these findings prompt further analyses on the relationship between irregular breaking waves and random wave overtopping, in order to establish appropriate Frequency Response Functions. These should involve the entire discharge signal instead of the mere average and more explanatory tools than the Fourier spectrum, such as the Wavelet Transform.

5.2. A prediction formula for breaking and non-breaking waves

The second part of the article proposes a predictive formula to estimate the mean overtopping discharge at vertical walls; a new parametrization has been introduced, where the dimensionless flow rate is consistent with that of Owen (1980), except for the foreshore slope, while $\zeta_{1/4}$ is used to obtain the relative crest freeboard (Eqs. (13) and (18)). Thus, the proposed formula accounts for the physics of the process by considering the main variables that affect the wave overtopping. The flow rate strictly depends on the water level at the toe of the structure, similar to the works that relate the discharge to a run-up level (Etemad-Shahidi et al., 2022; Yuhi et al., 2020; Hedge and Reis, 1998). However, it is worth specifying that $\zeta_{1/4}$ differs from a run-up height

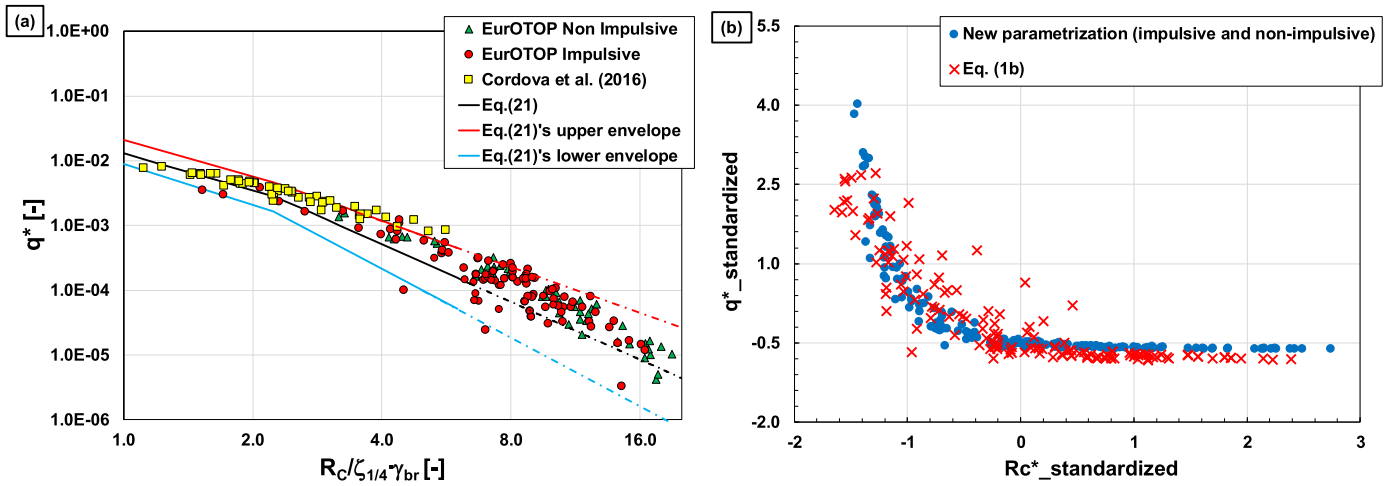

Fig. 14. New parametrization's performance. Panel (a): Eq. (21) vs. laboratory data. Broken lines indicate extrapolation from the boundaries of numerical tests; panel (b): comparison between new parametrization and EurOtop parametrization (Eq.(1b)). The axes plot the standardized non-dimensional variables.

since it was determined without the presence of the wall. Moreover, the formula includes the influence of the peak period; indeed, consistent with the literature (Lashley et al., 2021; Owen, 1980; Goda et al., 1975), a larger wave period produces a greater discharge. Finally, we have stressed the explicit role of the foreshore slope on the overtopping of vertical walls in very shallow water. As previously stated by Altomare et al. (2016) in their extensive analysis about the overtopping of sloping dikes with very shallow foreshores, the seabed slope seems to be a crucial variable that affects the overtopping in shallow water conditions, while its influence becomes weaker as deeper the waters. However, except for the Goda's model (2009), the predictive formulae for vertical seawalls do not consider the seabed slope's influence so far. EurOtop formulae neglect this variable (see Eq. (1)), while the deepwater-based-model of Lashley et al. (2021) takes it into account as the foreshore slope, along with h_{TOE}, would merely express the foreshore effect on the wave evolution process. Overall, this study differs from the existing empirical tools that relate the mean overtopping discharge either to the spectral wave conditions (H_{m0} and $T_{m-1,0}$) or to the wave run-up since it adopts a new hydraulic variable representing the upper tail of the distribution of wave displacements at the toe of the wall, $\zeta_{1/4}$. It is worth specifying that an interesting peculiarity of such a variable is that it can be determined using the same equation (Eq. (7)) both for a Gaussian wave process and a series of sinewaves.

The numerical analysis allowed us to collect a wide and varied dataset, encompassing three different planar beaches ($tan\alpha$) = 1/10 ÷ 1/50), a relative crest freeboard R_C^* that varies between 1.0 and 6.0 (different order of magnitude of the flow rate), and many water depths at the toe of the wall. A unique generalized formula has been derived that, through specific parameters (Eqs. (19,20)), is able to estimate the mean overtopping discharge of walls with different foreshore conditions, i.e. from shallow to extremely shallow waters.

A focus on uneven profiles has also been accomplished since the natural beaches are anything but uniform. A detailed analysis of convex and multi-slope foreshores allowed us to find out an equivalent slope necessary for estimating the flow rate at vertical seawalls in shallow water via Eq. (21). Although all four hypotheses of equivalent slope investigated (Section 4.3.1.) provide reasonable results, numerical outcomes indicate a sort of local slope at the toe of the structure as the equivalent slope, Eq. (22), which requires the identification of the scale parameter A that better describes the beach profile. On the other hand, in the case of a multi-slope foreshore like that of *NF_MT*, the local slope at the toe of the wall can be easily adopted. Nevertheless, the study reveals that the hypothetical slope recently suggested by Lashley et al. (2023) may be a valid alternative. Although the authors verified it on a single mildly-varying foreshore, its use gives satisfactory results. However, such a hypothetical slope has limited validity; it cannot be applied to seawalls located in shallow waters ($h_{TOE}/H_{m0,DEEP} \geq 1$), where the foreshore slope could still (slightly) affect the overtopping process.

Finally, we have verified our predictive tool with 194 laboratory data derived from different experimental campaigns on vertical walls in shallow waters. Specifically, the overtopping tests of the CLASH database classified as reliable (RF 1 and 2) and those carried out on the MT profile (Cordova et al., 2015; 2016) are used. Besides a slight bias, the predictive equation is quite consistent with physical model data, which indeed fall within the envelope's band of the numerical data. This corroborates the findings of Suzuki et al. (2017) and Buccino et al. (2023) that SWASH reproduces realistically the physics of the process, even if it tends to return some lower values of the flow rate. Nevertheless, the double-power law has been re-calibrated based on laboratory tests, Eq. (24). Such a comparison also highlights two main advantages of the new predictive tool: it significantly reduces the scatter of data compared to that of the EurOtop parametrization (Fig. 14) and is able to describe a unique behavior regardless of the loading conditions, i.e. impulsive or pulsating waves.

5.3. Limitation of the study and perspectives

The results of this study apply to vertical walls and long-crested wave spectra with a single peak in deep water. Along with the relative crest range $1 \leq R_c/\zeta_{1/4} \leq 6$, the use of $T_{p,DEEP}$ in the predictive equations would limit the application domain to the very shallow waters ($h_{TOE}/H_{m0,DEEP}$ larger than 0.3), where a certain amount of energy remains concentrated about the deep water peak. However, there is potential to extend those application boundaries. From one side, the fact that Buccino et al. (2003) found the experiments of van Gent (1999) reasonably consistent with those of the *Malecòn Tradicionàl* vertical seawall leads to imagine that the same variables, particularly $\zeta_{1/4}$, could predict the overtopping rate at sloping walls also. This deserves to be assessed in future research works. On the other side, numerical experiments carried out in this study under extremely shallow waters suggest that the new formulae can be surprisingly accurate even when the wave energy at the structure shifts almost completely to the low frequency domain. An example is given in Fig. 16 for two groups of experiments carried out on a slope 1:50. It can be seen that the data are equally well predicted by Eq. (21), either in the case of very ($h_{TOE}/H_{m0,DEEP} = 0.5$) or extremely shallow waters ($h_{TOE}/H_{m0,DEEP} = 0.2$).

Finally, the effects of short crestedness could be straightforwardly accounted for via the coefficients proposed by Altomare et al. (2020) in

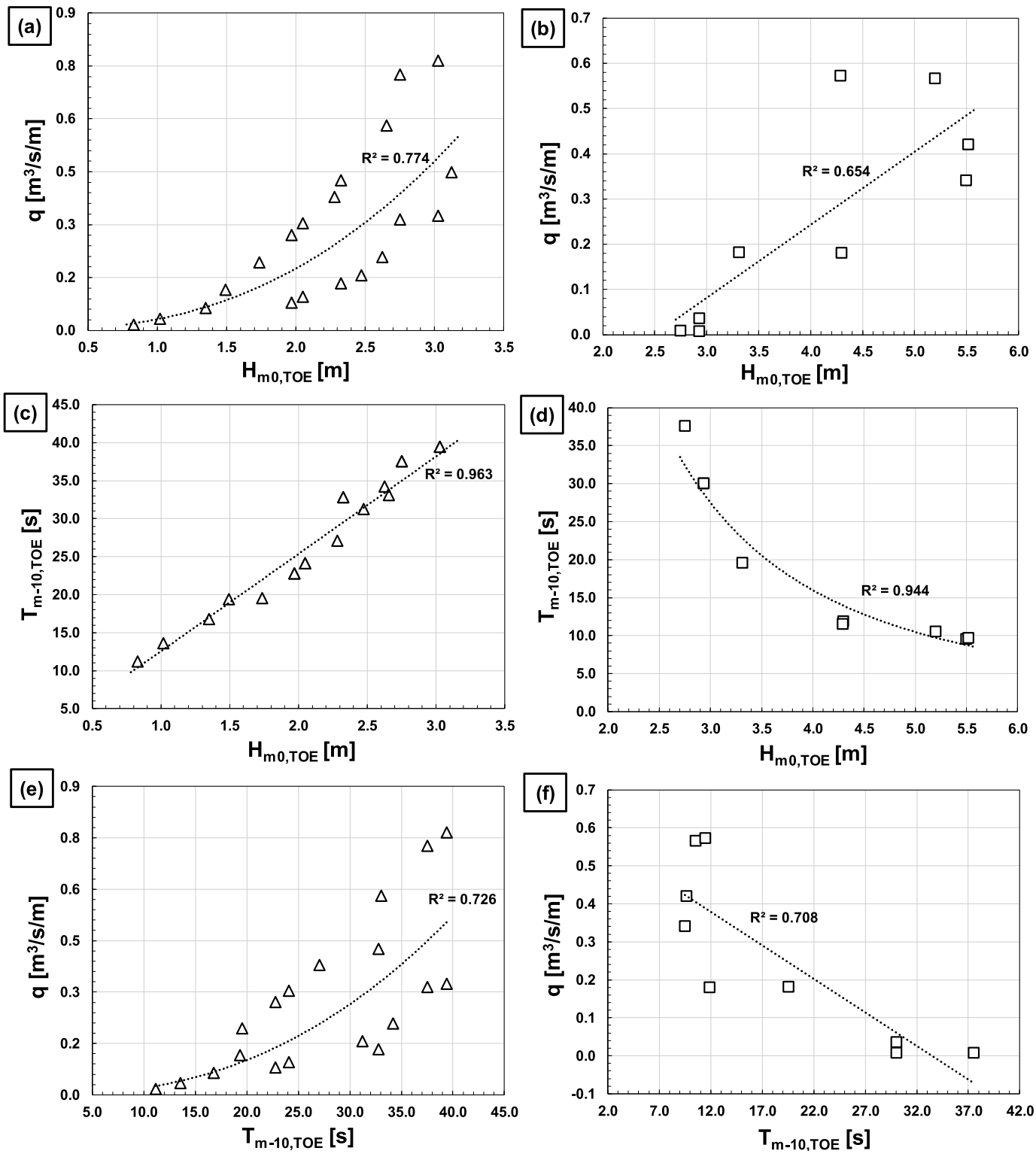

Fig. 15. Correlation plots. Panels (a), (c) and (e) depict random wave data of Fig. 6; panels (b), (d) and (f) refer to 9 data from the NF_U subset.

their study of sloping walls with shallow foreshores.

6. Conclusions

The work describes the analysis of the wave overtopping process at seawalls in shallow waters through an extensive numerical experimental campaign. In particular, the 232 tests performed via SWASH have allowed us to ascertain the main hydraulic variables involved in the overtopping process and to determine a more appropriate formulation for estimating the average flow rate.

Overall, the study confirms the capability of SWASH to adequately capture the physics that rules the overtopping process in shallow waters, as demonstrated by comparing the formula gathered with numerical data and 194 physical model tests. Indeed, despite a slight underestimation, the double power function appears well correlated to the laboratory data. Therefore, the numerical analysis performed in this work

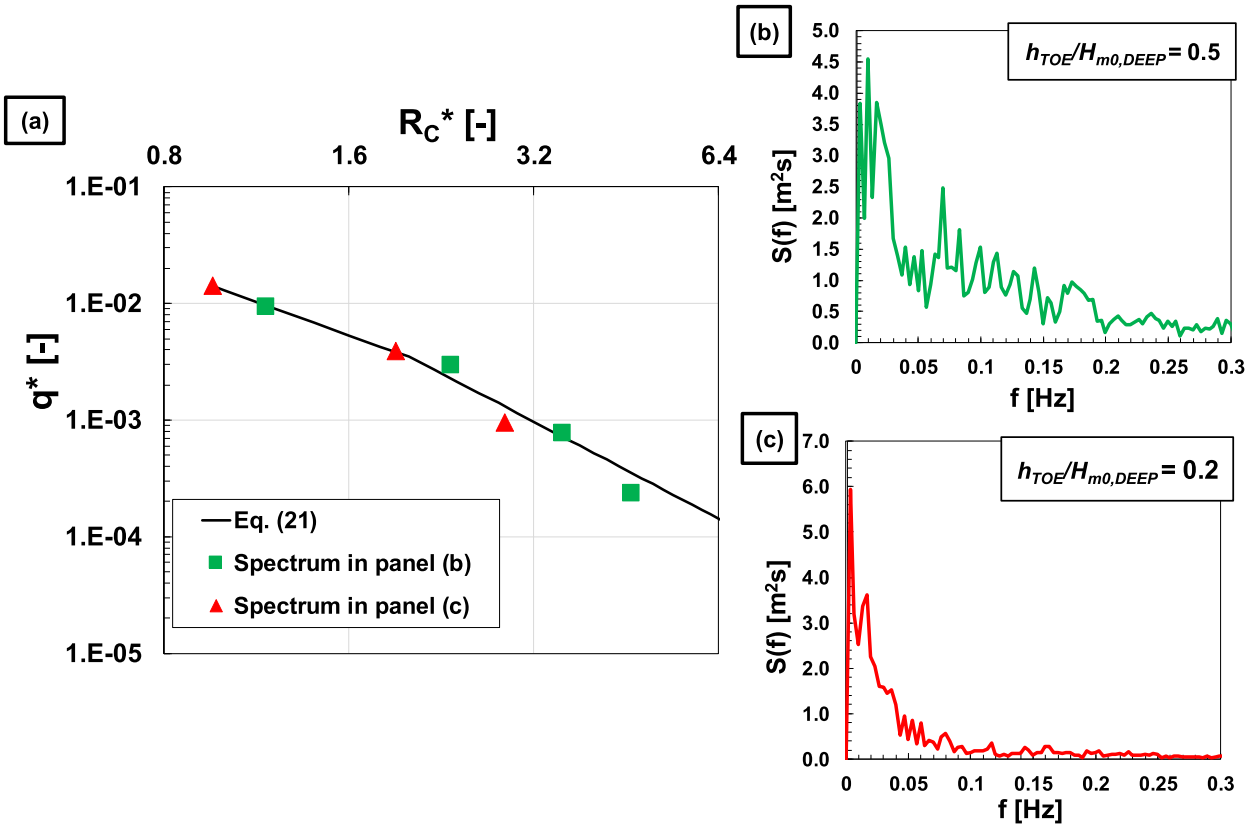

Fig. 16. Comparison between numerical shallow water experiments (spectrum in panel (b)) and extremely shallow water experiments (spectrum in panel (c)). The bottom slope is 1:50.

leads to reliable findings.

Based on two different types of experiments, the study has established that the energy distribution in the frequency domain does not affect the average flow rate. On the other hand, numerical results have confirmed the previous finding of Buccino et al. (2023), which demonstrated that the upper tail of wave displacement distribution actually impacts the overtopping process at a larger extent.

The double power function suggested to estimate the mean overtopping discharge – and re-calibrated based on the laboratory data – exhibits two main peculiarities:

- it yields a generalized formula for shallow waters conditions (i.e. hTOE/Hm0,DEEP < 4). Furthermore, unlike the EurOtop approach, it describes a unique behavior for breaking and non-breaking waves;
- the proposed parametrization considers the main features concerning the physics of the process, such as the influence of peak period or foreshore slope on the flow rate. An equivalent slope has been proposed in case of uneven seabed.

Finally, the proposed formula can potentially lead to a practical advantage for the engineering community that needs to be highlighted. Specifically, the hydraulic variable $\zeta_{1/4}$ required for estimating q may be inferred from wave setup and variance of the wave process, which, in turn, can be easily derived using either empirical models for regular bathymetries (almost uniform slope) or numerical models. The latter cannot necessarily be a phase-resolving model; in fact, phase-averaged models might prove suitable if it includes an empirical wave breaking model based on field data (e.g. Battjes and Stive,1978) that inherently accounts for the effects of surf beats. Future analysis might verify this issue.

CRediT authorship contribution statement

Sara Tuozzo: Software, Methodology, Investigation, Conceptualization. **Mario Calabrese:** Supervision, Formal analysis. **Mariano Buccino:** Methodology, Conceptualization.

Declaration of competing interest

The authors declare that they have no known competing financial interests or personal relationships that could have appeared to influence the work reported in this paper.

Data availability

We have shared our data in an ad-hoc table

Acknowledgements

The authors acknowledge the two anonymous reviewers for their stimulating comments that have significantly improved the article's clarity and quality. Also, the authors wish to gratefully acknowledge Ms Anna Rita Sabatino for her assistance in numerical testing.

Supplementary materials

Supplementary material associated with this article can be found, in the online version, at doi:10.1016/j.apor.2024.104009.

APPENDIX I. Grid sensitivity

To perform the numerical analysis described in this paper, we have discretized the horizontal domain in order to obtain 70 points for wave length (as mentioned in Section 3.1). However, the results should be affected by the grid size. To verify this issue, we have selected 9 experiments of *NF_U* and performed a grid sensitive analysis. These tests have been repeated with a coarser and a finer discretization. Specifically, we have doubled and halved the grid spacing, obtaining $L/\Delta x$ equals to 140 and 35, respectively. Fig. A.I.1.a plots the variation in the flow rate, expressed as the ratio between the mean overtopping discharge computed with the different grid size, q', and that obtained with $L/\Delta x = 70$. The coarser grid produces significant variations in the mean overtopping discharge, especially for low rates (Fig. A.I.1.b). On the other hand, the halved grid has not a significant effect; the discharges vary between +0.46 and -0.35 with regard to the original grid (+3% on average). These variation rates do not weigh more than the typical uncertainties related to the wave overtopping phenomena (e.g. Romano et al., 2015). Therefore, the discretization employed in this work assures that the obtained results are almost unaffected by the grid size.

It is worth noting that the grid sensitivity analysis only concerns the mean overtopping discharge; based on previous works' findings (Buccino et al., 2023; Suzuki et al., 2017), we can assume that the grid size has no much influence on wave evolution.

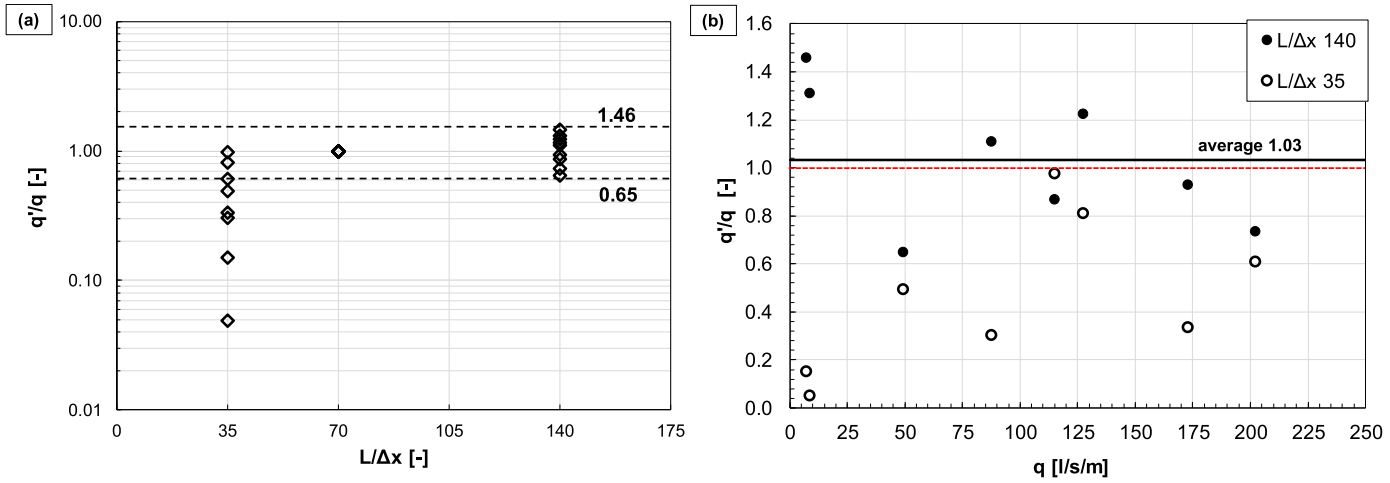

Fig. A.I.1. Variation in mean overtopping discharge due to the numerical discretization. Panel (a): variation vs grid point per wave length; panel (b): variation as a function of the flow rate.

APPENDIX II. Effects of spurious subharmonics in JONSWAP random wave generation

The essence of the analysis is that spurious subharmonics associated with linear generation in intermediate waters significantly affect the motion if the amount of long-wave energy generated in the flume exceeds the value predicted by the theory. This is consistent with Barthel et al. (1983).

Longuet-Higgins and Stewart (1962) showed that a periodic wave group propagating on a flat bottom forces a second order set-down long wave of amplitude:

$$\overline{\zeta} = \frac{S_{xx}}{\rho \cdot (gh - c_G^2)} = \left[\frac{g\left(1 + \frac{4kh}{senh(2kh)}\right)}{16\ (gh - c_G^2)} \right] \cdot H^2 = R_f \cdot H^2 \tag{A.II.1}$$

In which S_{xx} is the xx component of the radiation stress tensor, c_G is the group celerity, and R_f (in the square brackets) is a function of the wave frequency, f.

Therefore, for a narrow band process where the wave frequencies all equal the peak value f_p, we have:

$$m_{0,low} = VAR[\overline{\zeta}] = \left\{ \left[\frac{g\left(1 + \frac{4kh}{senh(2kh)}\right)}{16\ (gh - c_G^2)} \right]_{f=f_p} \right\}^2 \cdot VAR\left[H^2\right] = \left(R_{f_p}\right)^2 \cdot VAR\left[H^2\right] \tag{A.II.2}$$

in which *VAR* [*] denotes the statistical variance operator and R_{f_p} is calculated at the peak frequency. Eq. (A.II.2) is assumed as theoretical reference in the analysis.

For the tests *SSh_MT1* and *SSh_MT3*, we split long and short-wave signals at 20 positions along the horizontal part of the flume, using a Fourier filter with cut-off frequency $f_p/2$. Then, the short wave signal is zero-up crossed, and *VAR* [H^2] is calculated; of course, R_{f_p} is computed at the shortwave peak.

Fig. A.II.1, shows that the measured long-wave energy ($m_{0,low}$) remains mostly below the expected theoretical value, so excluding the presence of substantial parasitic sub-harmonics.

Conversely, BOUND generated waves (*SSh_MT2* and *SSh_MT3*) match reasonably well with Eq. (A.II.2), as shown in Fig. A.II.2. This was certainly expected, as the long wave component of Eq. (A.II.1) is provided at the generation boundary in the second term of Eq. (3).

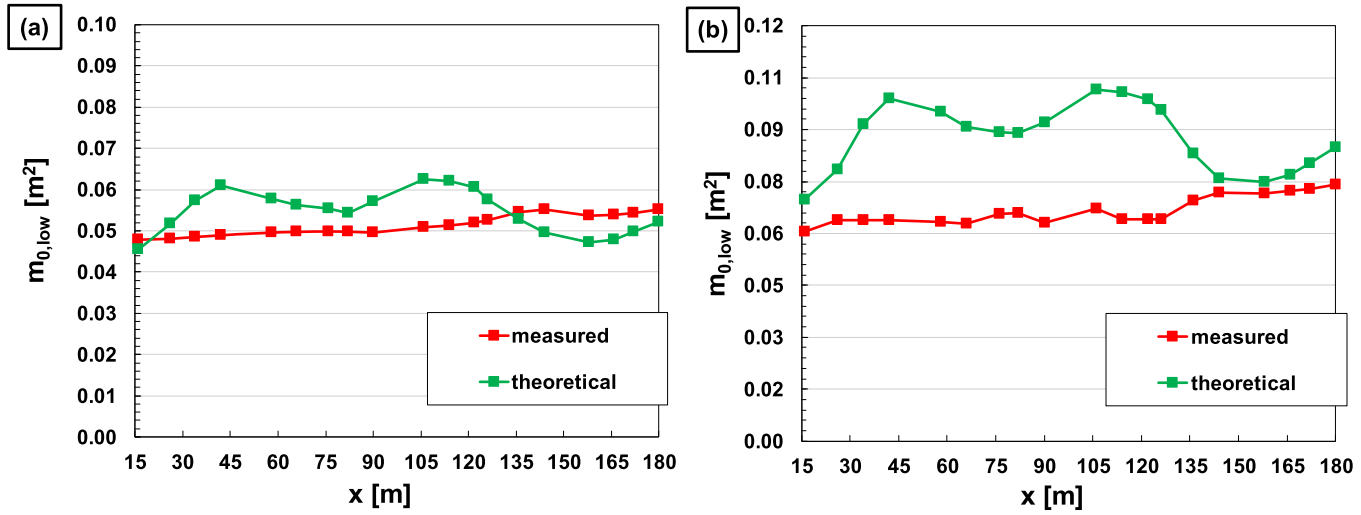

Fig. A.II.1. Panels (a) and (b) compare theoretical and measured $m_{0,low}$ for SSh_MT1 and SSh_MT3, respectively.

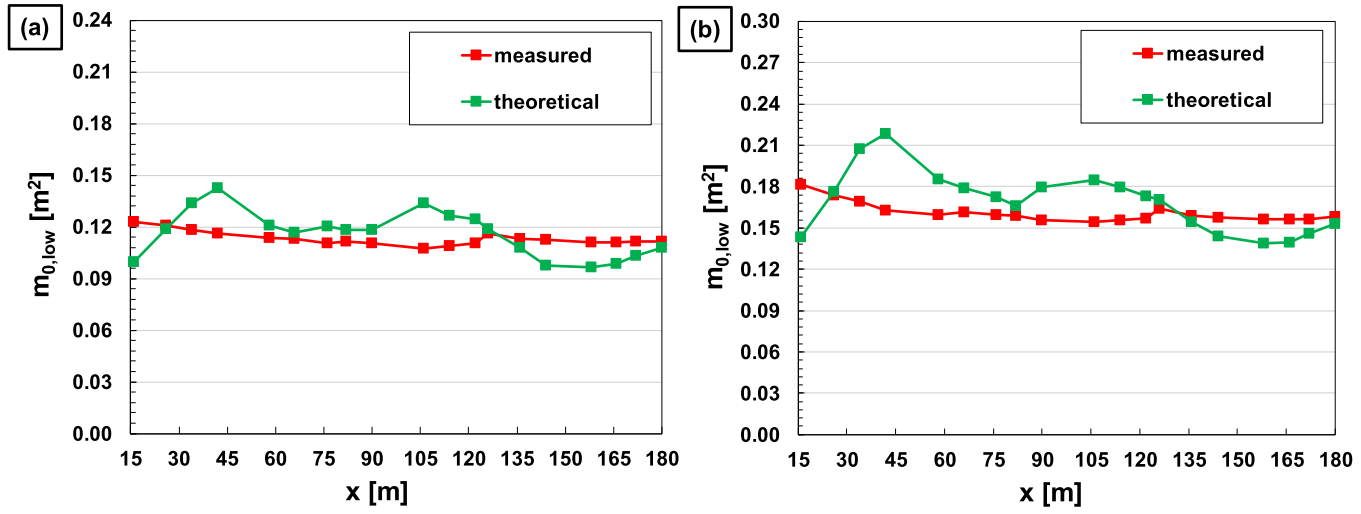

Fig. A.II.2. Panels (a) and (b) compare theoretical and measured $m_{0,low}$ for SSh_MT2 and SSh_MT4, respectively.

References

Allsop, W., Bruce, T., Pearson, J., Besley, P., 2005. Wave overtopping at vertical and steep seawalls. In: Proceedings of the Institution of Civil Engineers-Maritime Engineering, 158. Thomas Telford Ltd, pp. 103–114. https://doi.org/10.1680/maen.2005.158.3.103.

Altomare, C., Suzuki, T., Verwaest, T., 2020. Influence of directional spreading on wave overtopping of sea dikes with gentle and shallow foreshores. Coast. Eng. 157, 103654 https://doi.org/10.1016/j.coastaleng.2020.103654.

Altomare, C., Gironella, X., Crespo, A.J., 2021. Simulation of random wave overtopping by a WCSPH model. Appl. Ocean Res. 116, 102888 https://doi.org/10.1016/j.apor.2021.102888.

Barthel, V., Mansard, E.P.D., Sand, S.E., Vis, F.C., 1983. Group bounded long waves in physical models. Ocean Eng 10 (4), 261–294. https://doi.org/10.1016/0029-8018(83)90012-4.

Battjes, J.A., Janssen, J.P.F.M., 1978. Energy loss and set-up due to breaking of random waves. Coastal Engineering 1978, pp. 569–587.

Bertin, X., de Bakker, A., Van Dongeren, A., Coco, G., André, G., Ardhuin, F., Bonneton, P., Bouchette, F., Castelle, B., Crawford, W.C., Davidson, M., Deen, M., Dodet, G., Guérin, T., Inch, K., Leckler, F., McCall, R., Muller, H., Olabarrieta, M., Roelvink, D., Ruessink, G., Sous, D., Stutzmann, E., Tissier, M., 2018. Infragravity waves: from driving mechanisms to impacts. Earth-Sci. Rev. 177, 774–799. https://doi.org/10.1016/j.earscirev.2018.01.002.

Bruun, P., 1954. Coast Erosion and the Development of Beach Profiles, 44. US Beach Erosion Board.

Buccino, M., Del Vita, I., Calabrese, M., 2013. Predicting wave transmission past reef ball submerged breakwaters. J. Coast. Res. (65), 171–176. https://doi.org/10.2112/SI65-030.1.

Buccino, M., Di Leo, A., Tuozzo, S., Lopez, L.F.C., Calabrese, M., Dentale, F., 2023. Wave overtopping of a vertical seawall in a surf zone: a joint analysis of numerical and laboratory data. Ocean Eng 288, 116144. https://doi.org/10.1016/j.oceaneng.2023.116144.

Buckley, M.L., Lowe, R.J., Hansen, J.E., van Dongeren, A.R., Pomeroy, A., Storlazzi, C.D., Rijnsdorp, D.P., da Silva, R.F., Contardo, S., Green, R.G., 2022. Wave-driven hydrodynamic processes over fringing reefs with varying slopes, depths, and roughness: implications for coastal protection. J. Geophys. Res. Oceans 127. https://doi.org/10.1029/2022JC018857.

Chen, W., Warmink, J.J., Van Gent, M.R.A., Hulscher, S.J.M.H., 2021. Numerical modelling of wave overtopping at dikes using OpenFOAM®. Coast. Eng. 166, 103890 https://doi.org/10.1016/j.coastaleng.2021.103890.

De Rouck, J., Geeraerts, J., 2005. CLASH-final report: full scientific and technical report.

de Waal, J.P., Van der Meer, J.W., 1993. Wave runup and overtopping on coastal structures. Coastal Engineering 1992, pp. 1758–1771.

Dean, R.G., 1977. Equilibrium beach profiles: US Atlantic and Gulf coasts.

den Bieman, J.P., van Gent, M.R., van den Boogaard, H.F., 2021. Wave overtopping predictions using an advanced machine learning technique. Coast. Eng. 166, 103830 https://doi.org/10.1016/j.coastaleng.2020.103830.

Draper, N.R., Smith, N., 1998. Applied Regression Analysis 1–716. https://doi.org/10.1002/9781118625590.

Etemad-Shahidi, A., Koosheh, A., van Gent, M.R., 2022. On the mean overtopping rate of rubble mound structures. Coast. Eng. 177, 104150 https://doi.org/10.1016/j.coastaleng.2022.104150.

EurOtop, Van der Meer, J.W., Allsop, N.W.H., Bruce, T., De Rouck, J., Kortenhaus, A., Pullen, T., 2018. Manual on Wave Overtopping of Sea Defences and Related Structures. An overtopping Manual Largely Based On European research, but for Worldwide Application. Schüttrumpf.

Goda, Y., Kishara, Y., Kamiyama, Y., 1975. Laboratory Investigation On the Overtopping Rate of Seawalls By Irregular Waves. Report of the Port and Harbour Research Institute.
Goda, Y., 1995. Japan's Design Practice in Assessing Wave Forces on Vertical Breakwaters. Wave forces On Inclined and Vertical Wall Structures. ASCE, p. 402.
Goda, Y., 2009. Derivation of unified wave overtopping formulae for seawalls with smooth, impermeable surfaces based on selected CLASH datasets. Coast. Eng. 56, 385–399.
Gruwez, V., Altomare, C., Suzuki, T., Streicher, M., Cappietti, L., Kortenhaus, A., Troch, P., 2020. An inter-model comparison for wave interactions with sea dikes on shallow foreshores. J. mar. sci. eng. 8 (12), 985. https://doi.org/10.3390/jmse8120985.
Hasselmann, K., 1962. On the non-linear energy transfer in a gravity-wave spectrum Part 1. General theory. J. Fluid Mech. 12, 481–500.
Hasselmann, K., Barnett, T.P., Bouws, E., Carlson, H., Cartwright, D.E., Enke, K., Ewing, J.A., Gineapp, H., Hasselmann, D.E., Kruseman, P., Meerburg, A., Muller, P., Olbers, D.J., Richter, K., Walden, H., 1973. Measurements of Wind-Wave Growth and Swell Decay During the Joint North Sea Wave Project (JONSWAP). Ergaenzungsheft zur Deutschen Hydrographischen Zeitschrift, Reihe A.
Hansen, W., 1956. Theorie zur Errechnung des Wasserstandes und der Strömingen in Randmeeren nebst Anwendungen. Tellus 8, 289–300.
Hedges, T.S., Reis, M.T., 1998. Random wave overtopping of simple seawalls: a new regression model. Water Maritime Energy J., ICE 130, 1–10.
Henderson, C.S., Fiedler, J.W., Merrifield, M.A., Guza, R.T., Young, A.P., 2022. Phase resolving runup and overtopping field validation of SWASH. Coast. Eng 175, 104128. https://doi.org/10.1016/j.coastaleng.2022.104128.
Hofland, B., Chen, X., Altomare, C., Oosterlo, P., 2017. Prediction formula for the spectral wave period Tm-1,0 on mildly sloping shallow foreshores. Coast. Eng. 123, 21–28. https://doi.org/10.1016/j.coastaleng.2017.02.005.
Hughes, S.A., 2004. Estimation of wave run-up on smooth, impermeable slopes using the wave momentum flux parameter. Coast. Eng. 51 (11–12), 1085–1104. https://doi.org/10.1016/j.coastaleng.2004.07.026.
Ibrahim, M.S., Baldock, T.E., 2020. Swash overtopping on plane beaches–Reconciling empirical and theoretical scaling laws using the volume flux. Coast. Eng. 157, 103668.
Kraus, N.C., McDougal, W.G., 1996. The effects of seawalls on the beach: part I, an updated literature review. J. Coast. Res. 691–701.
Lam, D.C.L., Simpson, R.B., 1976. Centered differencing and the box scheme for diffusion convection problems. J. Comput. Phys. 220 (4), 486–500.
Lashley, C.H., Zanuttigh, B., Bricker, J.D., Van der Meer, J., Altomare, C., Suzuki, T., Roeber, V., Oosterlo, P., 2020. Benchmarking of numerical models for wave overtopping at dikes with shallow mildly sloping foreshores: accuracy versus speed. Environ. Model. Softw. 130, 104740 https://doi.org/10.1016/j.envsoft.2020.104740.
Lashley, C.H., van der Meer, J.W., Bricker, J.D., Altomare, C., Suzuki, T., Hirayama, K., 2021. Formulating wave overtopping at vertical and sloping structures with shallow foreshores using deep-water wave characteristics. J. Waterw. Port Coast. Ocean Eng. 147, 6. https://doi.org/10.1061/(ASCE)WW.1943-5460.0000675.
Lashley, C.H., Brown, J.M., Yelland, M.J., Van der Meer, J.W., Pullen, T., 2023. Comparison of deep-water-parameter-based wave overtopping with wirewall field measurements and social media reports at Crosby (UK). Coast. Eng. 179, 104241 https://doi.org/10.1016/j.coastaleng.2022.104241.
Nicolae Lerma, A., Pedreros, R., Senechal, N., 2016. Wave set-up and run-up variability on a complex barred beach during highly dissipative storm conditions. J. Coast. Res. 75, 882–886. https://doi.org/10.2112/SI75-177.1.
Longuet-Higgins, M.S., Stewart, R.W., 1962. Radiation stress and mass transport in gravity waves, with application to 'surf beats. J. Fluid Mech. 13 (4), 481–504. https://doi.org/10.1017/S0022112062000877.
Lopez, L.F.C., Salerno, D., Dentale, F., Capobianco, A., Buccino, M., 2015. Experimental campaign on the overtopping of the seawall Malecòn Tradicional. In: The Twenty-fifth International Ocean and Polar Engineering Conference. OnePetro, 2015.
Lopez, L.F.C., Salerno, D., Dentale, F., Capobianco, A., Buccino, M., 2016. Wave overtopping at Malecòn Tradicional, la Habana. Cuba. Coast. Eng. Proc. 2016 (35), 24. -24.
Losada, I.J., Lara, J.L., Guanche, R., Gonzalez-Ondina, J.M., 2008. Numerical analysis of wave overtopping of rubble mound breakwaters. Coast. Eng. 55 (1), 47–62. https://doi.org/10.1016/j.coastaleng.2007.06.003.
Mase, H., Tamada, T., Yasuda, T., Hedges, T.S., Reis, M.T., 2013. Wave runup and overtopping at seawalls built on land and in very shallow water. J. Waterw. Port Coast. Ocean Eng. 139 (5), 346–357. https://doi.org/10.1061/(ASCE)WW.1943-5460.0000199.
Nguyen, T.H., Hofland, B., Dan Chinh, V., Stive, M., 2020. Wave overtopping discharge for very gently sloping foreshores. Water (Basel) 12 (6), 1695. https://doi.org/10.3390/w12061695.
Oumeraci, H., Allsop, N.W.H., De Groot, M.B., Crouch, R.S., Vrijling, J.K., 1999. Probabilistic Design Tools for Vertical Breakwaters Balkema. Rotterdam, the Netherlands.
Owen, M.W., 1980. Design of seawalls allowing for wave overtopping. Hydraulics Research. Wallingford, Report No. EX 924, UK.
Pillai, K., Etemad-Shahidi, A., Lemckert, C., 2019. Wave run-up on bermed coastal structures. Appl. Ocean Res. 86, 188–194. https://doi.org/10.1016/j.apor.2019.02.006.
Rijnsdorp, D.P., Smit, P.B., Zijlema, M., 2014. Non-hydrostatic modelling of infragravity waves under laboratory conditions. Coast. Eng. 85, 30–42. https://doi.org/10.1016/j.coastaleng.2013.11.011.
Romano, A., Bellotti, G., Briganti, R., Franco, L., 2015. Uncertainties in the physical modelling of the wave overtopping over a rubble mound breakwater: the role of the seeding number and of the test duration. Coast. Eng. 103, 15–21. https://doi.org/10.1016/j.coastaleng.2015.05.005.
Schäffer, H., 1993. Infragravity waves induced by short-wave groups. J Fluid Mech 247, 551–588. https://doi.org/10.1017/S0022112093000564.
Symonds, G., Huntley, D.A., Bowen, A.J., 1982. Two-dimensional surf beat: long wave generation by a time-varying breakpoint. J. Geophys. Res. Oceans 87 (C1), 492–498. https://doi.org/10.1029/JC087iC01p00492.
Smit, P., Zijlema, M., Stelling, G., 2013. Depth-induced wave breaking in a non-hydrostatic, near-shore wave model. Coast. Eng. 76, 1–16. https://doi.org/10.1016/j.coastaleng.2013.01.008.
Smit, P., Janssen, T., Holthuijsen, L., Smith, J., 2014. Non-hydrostatic modeling of surf zone wave dynamics. Coast. Eng. 83, 36–48. https://doi.org/10.1016/j.coastaleng.2013.09.005.
Suzuki, T., Verwaest, T., Hassan, W., Veale, W., Reyns, J., Trouw, K., Troch, P., Zijlema, M., 2011. The applicability of SWASH model for wave transformation and wave overtopping: a case study for the Flemish coast. In: Proc. 5th Int. Conf. Advanced Computational Methods Engineering, Liège, Belgium, 14-17 November 2011.
Suzuki, T., Altomare, C., Verwaest, T., Trouw, K., Zijlema, M., 2014. Two-dimensional wave overtopping calculation over a dike in shallow foreshore by SWASH. In: ICCE 2014: Proceedings of 34th International Conference on Coastal Engineering, Seoul, Korea, 15-20 June 2014. Coastal Engineering Research Council.
Suzuki, T., Altomare, C., Veale, W., Verwaest, T., Trouw, K., Troch, P., Zijlema, M., 2017. Efficient and robust wave overtopping estimation for impermeable coastal structures in shallow foreshores using SWASH. Coast. Eng. 122, 108–123. https://doi.org/10.1016/j.coastaleng.2017.01.009.
Suzuki, T., Altomare, C., Yasuda, T., Verwaest, T., 2020. Characterization of overtopping waves on sea dikes with gentle and shallow foreshores. J. mar. sci. eng. 8 (10), 752. https://doi.org/10.3390/jmse8100752.
Suzuki, T., Altomare, C., Willems, M., Dan, S., 2023. Non-hydrostatic modelling of coastal flooding in port environments. J. mar. sci. eng. 11 (3), 575. https://doi.org/10.3390/jmse11030575.
Tonelli, M., Petti, M., 2013. Numerical simulation of wave overtopping at coastal dikes and low-crested structures by means of a shock-capturing Boussinesq model. Coast. Eng. 79, 75–88. https://doi.org/10.1016/j.coastaleng.2013.04.007.
Tucker, M.J., 1950. Surf beats: sea waves of 1 to 5 min. period. In: Proc. R. Soc. Lond. A, 202, pp. 565–573.
Van Dongeren, A.R.J.A., Battjes, J., Janssen, T., Van Noorloos, J., Steenhauer, K., Steenbergen, G., Reniers, A.J.H.M., 2007. Shoaling and shoreline dissipation of low-frequency waves. J. Geophys. Res. Oceans 112 (C2). https://doi.org/10.1029/2006JC003701.
Van Gent, M.R. 1999. Wave run-up and wave overtopping for double peaked wave energy spectra. H3351.
Vicinanza, D., Dentale, F., Salerno, D., Buccino, M., 2015. Structural response of seawave slot-cone generator (SSG) from random wave CFD simulations. In: ISOPE International Ocean and Polar Engineering Conference, 2015, June.
Zanuttigh, B., Formentin, S., Van der Meer, J.W., 2016. Prediction of extreme and tolerable wave overtopping discharges through an advanced neural network. Ocean Eng 127, 722. https://doi.org/10.1016/j.oceaneng.2016.09.032.
Zhang, N., Zhang, Q., Zou, G., Jiang, X., 2016. Estimation of the transmission coefficients of wave height and period after smooth submerged breakwater using a non-hydrostatic wave model. Ocean Eng 122, 202–214. https://doi.org/10.1016/j.oceaneng.2016.06.037.
Zhang, N., Zhang, Q., Wang, K.H., Zou, G., Jiang, X., Yang, A., Li, Y., 2020. Numerical simulation of wave overtopping on breakwater with an armor layer of accropode using SWASH model. Water (Basel) 12 (2), 386. https://doi.org/10.3390/w12020386.
Zijlema, M., Stelling, G.S., 2008. Efficient computation of surf zone waves using the nonlinear shallow water equations with non-hydrostatic pressure. Coast. Eng. 55, 780–790. https://doi.org/10.1016/j.coastaleng.2008.02.020.
Zijlema, M., Stelling, G., Smit, P., 2011. SWASH: an operational public domain code for simulating wave fields and rapidly varied flows in coastal waters. Coast. Eng. 58 (10), 992–1012. https://doi.org/10.1016/j.coastaleng.2011.05.015.